Available online at www.sciencedirect.com
ScienceDirect
Geochimica et Cosmochimica Acta 73 (2009) 4761–4791
Geochimica et Cosmochimica Acta
www.elsevier.com/locate/gca

Trace and minor elements in sphalerite: A LA-ICPMS study

Nigel J. Cook [a,*], Cristiana L. Ciobanu [b,c], Allan Pring [b,c,d], William Skinner [d], Masaaki Shimizu [e], Leonid Danyushevsky [f], Bernhardt Saini-Eidukat [g], Frank Melcher [h]

[a] Natural History Museum, University of Oslo, Boks 1172 Blindern, N-0318 Oslo, Norway
[b] South Australian Museum, North Terrace, Adelaide, SA 5000, Australia
[c] Department of Earth and Environmental Sciences, University of Adelaide, SA 5005, Australia
[d] Ian Wark Research Institute, University of South Australia, Mawson Lakes Campus, SA, Australia
[e] Department of Earth Sciences, University of Toyama, Japan
[f] CODES, University of Tasmania, Hobart, Tasmania, Australia
[g] Department of Geosciences, North Dakota State University, Fargo, ND 58105, USA
[h] Federal Institute for Geosciences and Natural Resources (BGR), D-30655 Hannover, Germany

Received 21 January 2009; accepted in revised form 13 May 2009; available online 21 May 2009

Abstract

Sphalerite is an important host mineral for a wide range of minor and trace elements. We have used laser-ablation inductively coupled mass spectroscopy (LA-ICPMS) techniques to investigate the distribution of Ag, As, Bi, Cd, Co, Cu, Fe, Ga, Ge, In, Mn, Mo, Ni, Pb, Sb, Se, Sn and Tl in samples from 26 ore deposits, including specimens with wt.% levels of Mn, Cd, In, Sn and Hg. This technique provides accurate trace element data, confirming that Cd, Co, Ga, Ge, In, Mn, Sn, As and Tl are present in solid solution. The concentrations of most elements vary over several orders of magnitude between deposits and in some cases between single samples from a given deposit. Sphalerite is characterized by a specific range of Cd (typically 0.2–1.0 wt.%) in each deposit. Higher Cd concentrations are rare; spot analyses on samples from skarn at Baisoara (Romania) show up to 13.2 wt.% ($Cd^{2+} \leftrightarrow Zn^{2+}$ substitution). The LA-ICPMS technique also allows for identification of other elements, notably Pb, Sb and Bi, mostly as micro-inclusions of minerals carrying those elements, and not as solid solution. Silver may occur both as solid solution and as micro-inclusions. Sphalerite can also incorporate minor amounts of As and Se, and possibly Au (e.g., Magura epithermal Au, Romania). Manganese enrichment (up to ~4 wt.%) does not appear to enhance incorporation of other elements. Sphalerite from Toyoha (Japan) features superimposed zoning. Indium-sphalerite (up to 6.7 wt.% In) coexists with Sn-sphalerite (up to 2.3 wt.%). Indium concentration correlates with Cu, corroborating coupled $(Cu^{+}In^{3+}) \leftrightarrow 2Zn^{2+}$ substitution. Tin, however, correlates with Ag, suggesting $(2Ag^{+}Sn^{4+}) \leftrightarrow 3Zn^{2+}$ coupled substitution. Germanium-bearing sphalerite from Tres Marias (Mexico) contains several hundred ppm Ge, correlating with Fe. We see no evidence of coupled substitution for incorporation of Ge. Accordingly, we postulate that Ge may be present as Ge^{2+} rather than Ge^{4+}. Trace element concentrations in different deposit types vary because fractionation of a given element into sphalerite is influenced by crystallization temperature, metal source and the amount of sphalerite in the ore. Epithermal and some skarn deposits have higher concentrations of most elements in solid solution. The presence of discrete minerals containing In, Ga, Ge, etc. also contribute to the observed variance in measured concentrations within sphalerite.

1. INTRODUCTION

Sphalerite is the chief ore of zinc in all sulfide-rich base metal deposits. The simple formula, ZnS, belies the minerals' ability to incorporate a broad range of trace elements,

* Corresponding author.
E-mail address: nigelc@nhm.uio.no (N.J. Cook).

0016-7037/$ - see front matter © 2009 Elsevier Ltd. All rights reserved.
doi:10.1016/j.gca.2009.05.045

often at levels that are economic to exploit or pose an environmental hazard. In a number of Zn deposits, sphalerite is the main carrier of by-product Ga (Moskalyk, 2003), Ge (Höll et al., 2007) and In (Alfantazi and Moskalyk, 2003) – and more rarely of other valuable elements such as Ag. Deleterious elements may also be significantly concentrated within sphalerite, notably Cd, but also Mn, Hg, As, Tl, etc. If the Cd concentration is sufficiently high, it can be economically exploited as a by-product; giant Zn–Pb deposits such as Red Dog (Alaska) meet much of demand for the element. The broad range of trace element incorporation in sphalerite correlates with the color shown by natural specimens, which ranges from white, yellow, brown, red, pink, green, gray-black and black. A dark black color ('*marmatite*') normally indicates high Fe content (∼>6 wt.%), but other elements (e.g., Mn, Co) are also highly influential on color.

Many dozens of papers have dealt with aspects of sphalerite geochemistry. The pioneering work of Oftedahl (1940) showed how the sphalerite formation temperature is reflected by the trace element content. Cobalt and In are concentrated in hypo- and mesothermal ores, Ga and Ge (Hg and Sn) in lower-temperature ores; formation temperatures for Ge-rich sphalerite are lower than those for Ga-rich sphalerite. These early studies showed how In contents are lowest in Ga–Ge-enriched ores. Some older papers claiming high concentrations of a range of minor and trace elements have been partially discredited as electron beam techniques have replaced wet chemistry, showing the presence of μm-scale inclusions hosting the supposed trace elements. Despite this, uncertainties persist on the real range of minor and trace element concentrations in the sphalerite lattice itself, since it is not always possible to discriminate, even at the scale of an electron microprobe beam, between lattice-hosted elements and those in nano- and micro-scale inclusions, especially for sphalerite within fine-grained ores. Modern microanalytical techniques such as laser-ablation inductively coupled mass spectroscopy (LA-ICPMS), particle-induced X-ray emission spectrometry (PIXE), secondary ion mass spectroscopy (SIMS), etc. provide an opportunity not only to determine concentrations at detection limits lower than that of the electron microprobe, but they also provide direct or indirect information on whether a given trace element is present within the sulfide matrix or as micro- or submicroscopic inclusions of a different mineral since the latter, if sufficiently large, will be visible on the ablation profile. The volume of material analyzed by the LA-ICPMS technique is greater than that of the electron microprobe; spot size in this study ranges in size from 25 to 80 μm. This greater volume offers the advantage that any inhomogeneities present may be smoothed out, but does not allow analysis of those inhomogeneities, such as compositional zoning or fine intergrowths. Wavelength-dispersive electron microprobe analysis, even though the analyzed volume is smaller, also does not prevent analysis of an inhomogeneous volume, since compositional zoning and intergrowths commonly extend well below the 1–5 μm scale of the electron probe beam. Both methods are useful and complementary to one another. LA-ICPMS has been shown to be an efficient, accurate method for determination of trace element concentrations in sulfides (e.g., Watling et al., 1995; Cook et al., 2009) and comparable compounds (Ciobanu et al., 2009). LA-ICPMS has been frequently applied to problems such as concentrations of so-called invisible gold in pyrite and arsenopyrite, as well as to aspects of ore deposit formation (e.g., Butler and Nesbitt, 1999). Relatively few studies have used the method specifically regarding trace elements in sphalerite despite the excellent suitability of the method (e.g., Axelsson and Rodushkin, 2001).

In this study, we use *in situ* laser-ablation inductively coupled mass spectroscopy (LA-ICPMS) in a series of well characterized case studies of the concentrations of a range of minor and trace elements in a range of natural sphalerites. We aim to constrain the reasons for minor and trace element substitution, ranges of solid solution in natural samples, and the possible geological controls on sphalerite geochemistry. Due to the limitations of the LA-ICPMS technique identified above, we did not expressly set out to look at the smallest-scale structures in the analyzed samples. Our aim is to identify the range of concentrations in natural specimens and to analyze trends, in terms of inter-element correlations in a given sample, as well as systematic variations with respect to deposit type and geological provenance. Our dataset purposely includes several unusual sphalerites with concentrations of Mn, Cd and In at >1 wt.% levels. Investigation of such 'extreme' sphalerites was aimed at aiding understanding of substitution mechanisms at high concentrations.

The growing interest in the characteristics and phase relationships of ZnS, CdS, CdSe and other sphalerite-related structures (e.g., $CuInS_2$, $CuInSe_2$, Cu_2ZnSnS_4), stems from their applications as semi-conductors, solar cells, etc. The purity of these compounds, even at lowest concentrations, is both of interest and concern to the materials science community (e.g., Barreau, 2008).

2. BACKGROUND

In order to discuss and evaluate the new data in the context of sphalerite crystal chemistry, natural solid solutions and phase relationships, we include a background section, in which published minor/trace element data for sphalerite and information on mechanisms of trace element incorporation are reviewed.

Sphalerite is by far the most common of the three ZnS polymorphs and is isostructural with diamond, crystallizing as a face-centered cubic lattice with tetrahedrally-coordinated Zn and S ions. Wurtzite and matraite are hexagonal and trigonal ZnS polymorphs, respectively. Relationships between sphalerite and wurtzite may be complex, with the two minerals occasionally occurring together within intergrown aggregates (e.g., Minčeva-Stefanova, 1993). Nitta et al. (2007) have suggested that matraite, much rarer than either sphalerite or wurtzite, may not be a distinct mineral, but rather (1 1 1)-twinned sphalerite characteristic of high-temperature volcanic sublimates. Minerals of the sphalerite group, related minerals and others referred to in this paper are given, with formulae, in Table 1. The number of species fully isostructural with sphalerite that exist as minerals is

Table 1
Glossary of minerals in the sphalerite group and other species discussed in this paper.

Sphalerite group (Cubic, $F\bar{4}3m$)		**Space and point**	**groups**
Sphalerite	(Zn,Fe)S	$F\bar{4}3m$	$\bar{4}3m$
Hawleyite	CdS	$F\bar{4}3m$	$\bar{4}3m$
Metacinnabar	HgS	$F\bar{4}3m$	$\bar{4}3m$
Stilleite	ZnSe	$F\bar{4}3m$	$\bar{4}3m$
Tiemannite	HgSe	$F\bar{4}3m$	$\bar{4}3m$
Coloradoite	HgTe	$F\bar{4}3m$	$\bar{4}3m$
Related compound			
Polhemusite	(Zn,Hg)S	$P4/n$	$4/m$
Wurtzite group (Hexagonal, $P6_3mc$)			
Wurtzite	(Zn,Fe)S	$P6_3mc$	$6mm$
Greenockite	CdS	$P6_3mc$	$6mm$
Cadmoselite	CdSe	$P6_3mc$	$6mm$
Rambergite	MnS	$P6_3mc$	$6mm$
Related compound			
Matraite	ZnS	$R3m$	$3m$
Chalcopyrite group			
Chalcopyrite	$CuFeS_2$	$I\bar{4}2d$	$\bar{4}2m$
Gallite	$CuGaS_2$	$I\bar{4}2d$	$\bar{4}2m$
Roquesite	$CuInS_2$	$I\bar{4}2d$	$\bar{4}2m$
Laforetite	$AgInS_2$	$I\bar{4}2d$	$\bar{4}2m$
Stannite group			
Sakuraiite	$(Cu,Zn,Fe,In,Sn)_4S_4$	$P432$, $P\bar{4}3m$ or $Pm3m$	
Petrukite	$(Cu,Fe,Zn)_2(Sn,In)S_4$	$Pmn2_1$	$mm2$
Galena group			
Alabandite	MnS	$Fm3m$	$4/m\ \bar{3}2/m$
Stannite group			
Stannite	$Cu_2(Fe,Zn)SnS_4$	$I\bar{4}2m$	$\bar{4}2m$
Pirquitasite	Ag_2ZnSnS_4	$I\bar{4}2m$	$\bar{4}2m$
Kësterite	$Cu_2(Zn,Fe)SnS_4$	$I\bar{4}$	$\bar{4}$

limited to the Cd and Hg analogs, hawleyite (CdS) and metacinnabar (HgS), the selenides stilleite (ZnSe) and tiemannite (ZnSe) and the telluride coloradoite (HgTe).

Minor and trace element substitution in sphalerite is largely governed by the similarity of the size of a relatively large number of other ions to that of tetrahedrally-coordinated Zn^{2+}, as well as their affinity for tetrahedral coordination. The chemical structure of ZnS doped with Fe^{2+}, Cd^{2+} and other bivalent cations is discussed by Vaughan and Rosso (2006); see also Hotje et al. (2003). Elements which substitute for S include Se and As. The following sections summarize previous work that documents concentrations of, and substitution mechanisms for, specific minor and trace elements.

2.1. Element trends

Iron is almost always present in natural sphalerite; concentrations range from trace levels up to more than 15 wt.%. Lepetit et al. (2003) noted the solubility limit of FeS in ZnS as 52, 21 and 20 mol.% FeS at 700 °C for the Fe/FeS, $Fe_{0.97}S$ and Fe_{1-x}/FeS_2 buffers, respectively. The Fe content of sphalerite has been widely used as a geological barometer, with wide application to determination of formation conditions of metamorphosed and metamorphogenic ore deposits (e.g., Scott and Barnes, 1971; Scott, 1973; Lusk and Ford, 1978; Lusk et al., 1993; Martín and Gil, 2005), even if there are restrictions to the applicability of the method (e.g., Cook et al., 1994). Recently, Pring et al. (2008) have shown that substitution of Zn^{2+} by Fe^{2+} creates very little distortion of the sphalerite structure, even if there is some change in the cell parameters; clustering of Fe^{2+} within the structure is not favored. Lepetit et al. (2003) have discussed the possible role of Fe^{3+} and associated metal vacancies in Fe-rich sphalerite and related this to higher fS_2 at concentrations above 10 mol.% FeS.

Manganese concentrations of a few hundred to a few thousand ppm, often displaying considerable variation within hand sample or outcrop, are common in natural sphalerite (e.g., Graeser, 1969). Manganese incorporation takes place by simple cation exchange ($Zn^{2+} \leftrightarrow Mn^{2+}$); alabandite (MnS) is, however, not isostructural with sphalerite (galena structure). Concentrations of Mn at >2 wt.% levels, as documented in this study, are rarer, and approach the upper limit of MnS incorporation in the sphalerite structure (ca. 7 mol.% MnS; Sombuthawee et al., 1978). Above this limit, crystals adopt the wurtzite structure or contain separate domains of sphalerite and wurtzite, with solid solution of MnS in ZnS reaching 50 mol.% (Kaneko et al., 1984). Olivo and Gibbs (2003) have described exceptionally Mn-rich sphalerite ($Zn_{0.67-0.73}Mn_{0.21-0.25}Fe_{0.06-0.09}S$) coexisting with alabandite from Santo Toribio, Peru. Di Benedetto et al. (2005), drawing on an earlier identifying nanoclusters of Mn in sphalerite (Bernardini et al., 2004) have shown that the presence of Cd may influence the distribution of both Fe and Mn, with Mn and Fe typically inversely correlating with one another due to competition at the mineral–fluid interface.

The *cobalt* ion is similar in size to that of Fe and therefore sphalerite should commonly contain high concentrations of cobalt. Phase diagrams (e.g., Becker and Lutz, 1978) suggest extensive CoS–ZnS solid solution, with a phase of intermediate composition, $Zn_{30}Co_{20}S_{50}$ (40 mol.% CoS) confirmed to have the sphalerite structure. Relatively little data quantitative exist on Co concentrations in sphalerite, yet it is well known that Co-bearing sphalerite has a characteristic green color. Gem-quality green sphalerite specimens are known from Kipushi Mine, D.R. Congo. Intiomale and Oosterbosch (1974) state that Co contents of Kipuchi sphalerite ranged from 20 to 820 ppm; green varieties also contain Cu. Hofmann and Henn (1984) confirmed that the green color is due to the presence of Co, analyzing 840 ppm in one gem-quality specimen. Rager et al. (1996) have shown that as little as 100 ppm Co may change the optical properties of the mineral.

There are only limited data suggesting that sphalerite may accommodate significant concentrations of *nickel*. Despite a high detection limit (350–500 ppm), Huston et al. (1995) were able to report concentrations as high as 2000 ppm in sphalerite from Australian VHMS deposits. This was attributed to lattice-bound Ni rather than

inclusions. Solid solution up to 3 atom.% Ni is suggested by Wu et al. (1989) who were able to confirm the sphalerite structure of a $Ni_2S_{50}Zn_{48}$ phase.

Conventionally, *copper* (as Cu^{2+}) is not considered to be readily incorporated into the sphalerite structure in significant quantities (Craig, 1973), unless as part of a coupled substitution (see below). Instead, so-called "chalcopyrite disease" (generally sub-5 μm blebs of chalcopyrite, where Cu carries a single positive charge) appears as the host sphalerite cools (e.g., Barton and Bethke, 1987). These excretions are typically observed along crystallographic axes or twin boundaries. Sugaki et al. (1987) showed that the bulk chemical composition of sphalerite containing chalcopyrite disease falls well outside the limited solid solution field of Cu in the system CuS–FeS–ZnS (Kojima and Sugaki, 1984), even at temperatures as high as 800 °C, suggesting that simple exsolution can be ruled out.

There is probably more data on *cadmium* concentrations in sphalerite than any other element. Sphalerite is the chief ore of Cd, with extensive solid solution documented at higher-temperature (Chen et al., 1988). Cadmium-bearing sphalerite in abandoned mines and tailings dumps can represent a major environmental hazard (e.g., Schwartz, 2000; Piatak et al., 2004). Cadmium contents are commonly rather uniform in a given deposit, typically within the 0.1–.5 wt.% range; sometimes higher, especially in some Mississippi Valley type (MVT) deposits. Kelley et al. (2004) document Cd concentrations in stage I–IV sphalerite at Red Dog, Alaska (0.4–0.6 wt.%), which do not significantly diverge from one another, even though concentrations of other elements (Fe, Co, Mn, Tl and Ge) vary greatly in the different sphalerite generations in the deposit. Some authors have sought to show that the Cd/Zn ratio can efficiently discriminate between different genetic deposit types (e.g., Qian, 1987) or show how the Cd/Zn ratio can track changes in ore/fluid interaction in a given ore deposit (e.g., Gottesmann and Kampe, 2007; Gottesmann et al., 2009).

Several authors have suggested that significant amounts of *silver* may be incorporated in the sphalerite lattice (e.g., Taylor and Radtke, 1969). Although sometimes regarded as an Ag-carrier, practice indicates that higher concentrations are almost always related to microscopic or submicroscopic inclusions of discrete Ag-minerals. Nevertheless, concentrations up to 100 ppm, rarely more, are reported for a small number of ore deposits (e.g., Red Dog, Alaska; Kelley et al., 2004). Cabri et al. (1985) give values from less than the detection limit (<mdl) (i.e., 12 ppm) to 308 ppm for 'C' ores from Kidd Creek, but <mdl for Mattagami and Geco. An exception to the generally low Ag contents is the range of concentrations of 650–700 ppm obtained by the same authors for sphalerite from Nanisivik, N.W.T., Huston et al. (1995, 1996) report low levels of Ag in the sphalerite lattice of Australian ores, although reaching 30–110 ppm in the Agincourt deposit. Chryssoulis and Surges (1988) demonstrated, using ion microprobe techniques, that ppm levels of Ag within sphalerite make it a minor Ag-carrier in mill circuits at Brunswick, NB, Canada. Microanalysis of sphalerite often reveals heterogeneous distributions within individual datasets reflecting the significance of (micro)inclusions of Ag-minerals.

Although no phase diagram is available to support extensive solid solution, sphalerite may, apparently, host more than a few ppm *molybdenum*, although this is uncommon. Sphalerite in each of the five deposits studied by Huston et al. (1995) contained statistically significant concentrations (median from 15 to 95 ppm). The Waterloo and Agincourt deposits (greenschist facies) contained the highest Mo concentrations. Huston et al. (1995) believed these data did not reflect micro-inclusions of molybdenite, but rather substitution of Mo^{3+} into the lattice. Molybdenum concentrations of ca. 5000 ppm have been measured in sphalerite from black shale deposits, Yukon (Orberger et al., 2003).

Mercury-bearing sphalerite has been reported from various localities. In some deposits, the Zn-sulfide may be the dominant Hg-carrier. Exceptionally high contents of 0.08–16.35 wt.% Hg are reported from the Eskay Creek deposit (BC, Canada) by Grammatikopoulos et al. (2006). Samples highest in Hg are characterized by an abundance of Hg-bearing tetrahedrite, cinnabar and other sulfides, with the highest Hg concentrations measured in low-Fe-sphalerite. Direct substitution of Hg^{2+} for Zn^{2+} is invoked. There are no strong correlations between the concentrations of Hg and those of Fe, Zn, or Mn.

Sphalerite is not as a significant host for lattice-bound *gold*. Sphalerite is, however, commonly encountered as a host for particulate native gold/electrum, particularly in deposits that have undergone syn-metamorphic remobilization (e.g., Hurley and Crocket, 1985), and the assemblages contain abundant sulfosalts and/or tellurides.

Sphalerite is an important source of *gallium*, second only to bauxite ores (Moskalyk, 2003). Krämer et al. (1987) show up to 20 mol% Ga_2S_3 solid solution in sphalerite. Gallium concentrations tend to be higher in low-temperature, carbonate-hosted replacement deposits. Moskalyk (2003) states that Zn ores from some Mississippi Valley type deposits in the USA contain 50 ppm Ga. Melcher et al. (2006) compiled data for Ga concentrations in sphalerite from a number of Namibian Pb–Zn deposits, indicating concentrations at the several hundreds of ppm level in the main sphalerite generation at Khusib Springs and 2000–3120 ppm in very low-Fe-sphalerite from the Tsumeb ore. Rambaldi et al. (1986) report concentrations of 2.1–3.7 wt.% Ga in sphalerite from a sulfide nodule within a chondrite, concordant with the high solubility and complete solid solution determined experimentally at elevated temperatures (Krämer et al., 1987; Ueno and Scott, 1991).

Indium-bearing sphalerite has been widely reported (e.g., Burke and Kieft, 1980; Pattrick et al., 1993; Schwarz-Schampera and Herzig, 2002; Ishihara and Endo, 2007) and there is believed to be extensive solid solution between sphalerite and roquesite, $CuInS_2$ (Sombuthawee et al., 1978; Sombuthawee and Hummel, 1979; Parasyuk et al., 2003). Solid solution cannot, however, be complete because the two minerals have different crystallography, necessitating phase transition mid-way along the series. Shimizu et al. (2007), however, suggest the existence of solid solution between sphalerite and sakuraiite ($CuZn_2InS_4$; Kato, 1965; see also Kissin and Owens, 1986; Shimizu et al., 1986), but not between sakuraiite and roquesite. Indium is

incorporated within sphalerite via a coupled substitution ($Cu^{+}In^{3+}$) ↔ (Zn^{2+}, Fe^{2+}). Schorr and Wagner (2005) offered insights into the crystal chemistry of the sphalerite–roquesite solid solution, albeit working on synthetic rather than natural compounds. Several recent publications discussed the role played by In-bearing sphalerite. Sinclair et al. (2006) addressed the mineralogy of the Mount Pleasant In-bearing vein, replacement and breccia-hosted tin-base metal deposits (NB, Canada), where In is concentrated in sphalerite. Electron microprobe data for In range from <0.01 to 6.90% In. Sinclair et al. (2006) cite a mean content of 1.23 wt.%, but attribute the highest In levels to exsolution of discrete inclusions of In-rich minerals. Seifert and Sandmann (2006) undertook microprobe determinations of sphalerite from the German Erzgebirge. Iron-rich sphalerites are characterized by In contents from 0.03 to 0.38 wt.%. A negative correlation exists between (Zn + Fe) and In, said to reflect structural substitution of In in sphalerite. Murao et al. (2008) examined In-bearing ores in Japan and India, noting up to 1.89 wt.% In from Goka, Japan.

The majority of world *thallium* production is derived from zinc smelting (Nriagu, 1998), suggesting that sphalerite is a major host for the element. Little quantitative data, however, exist. Murao et al. (1996) mention 13 ppm Tl in sphalerite from Japanese Kuroko ores, with the element preferentially found in coexisting pyrite. Kelley et al. (2004) gives data for Tl at Reg Dog, showing that concentrations sequentially decrease with deposition from 126 ppm in early brown sphalerite, although up to 355 ppm Tl is reported from latest tan-colored sphalerite. Xiong (2007) mentions the possibility of Tl incorporation in sphalerite in terms of $Tl^{+}_{0.5}As^{3+}_{0.5}S$ solid solution.

Sphalerite (and wurtzite) are by far the most important economic sources of *germanium*. The element may, in some cases, be enriched in the Zn-sulfide up to as much as 3000 ppm (Bernstein, 1985). Microanalytical data have been reviewed by Höll et al. (2007). Germanium would appear to be preferentially concentrated in low-Fe-sphalerite (Johan et al., 1983; Johan and Oudin, 1986; Johan, 1988; Cassard et al., 1996). There is no evidence for direct substitution of Zn^{2+} by Ge^{2+} in sphalerite and wurtzite (Bernstein, 1985; Johan, 1988; Möller and Dulski, 1993). The presence of other elements, e.g., Ag, Cu, would appear to enhance incorporation (Moh and Jäger, 1978). Johan (1988) accordingly proposed a general coupled substitution mechanism for trivalent and tetravalent elements (including Ge^{4+}), in sphalerite, expressed in the following substitutions: $2M^{+} + M^{2+} + M^{4+} \leftrightarrow 4Zn^{2+}$; and $(x + 2y)M^{+} + yM^{2+} + xM^{3+} + yM^{4+} \leftrightarrow (2x + 4y)Zn^{2+}$, where $M^{+} = Ag^{+}$, Cu^{+}; $M^{2+} = Cu^{2+}$, Fe^{2+}, Cd^{2+}, Mn^{2+}, Hg^{2+}; $M^{3+} = In^{3+}$, Ga^{3+}, Fe^{3+}, Tl^{3+}; $M^{4+} = Ge^{4+}$, Sn^{4+}, Mo^{4+}, W^{4+} and x and y are atomic proportions of M^{3+} and M^{4+}, substituting for Zn^{2+}, respectively. The two substitutions above indicate that incorporation of M^{3+} and M^{4+} into sphalerite is possible due to formation of donor–acceptor pairs with monovalent ions (Johan, 1988). Incorporation of trace elements into the structure of sphalerite, including Ge, is likely to depend upon the diffusion/growth velocity ratio. In situ SIMS analysis of banded Zn-sulfides indicates that there are positive correlations between Ge, Tl, As, Fe, and Pb (Pimminger et al., 1985). Möller (1987) suggested that the content of Ge in hydrothermal fluids depends on the leaching temperature, and be roughly indicated by the Ga/Ge ratio in sphalerite. Mladenova and Valchev (1998) proposed that the Ga/Ge ratio in sphalerite could be used as a temperature indicator for hydrothermal fluids in the carbonate-hosted Sedmochislenitsi Deposit, Bulgaria. Melcher et al. (2006) determined concentrations of Ge in sphalerite from Khusib Springs, Namibia, to be generally <30 ppm, lower than the <30–68 ppm determined in the Tsumeb deposit (70–140 ppm; Lombaard et al., 1986) or 8–427 ppm in other deposits of the Otavi Mountain Land (Emslie and Beukes, 1981).

There are few accounts of elevated concentrations of *tin* in sphalerite and little support for solid solution of Sn in sphalerite (Moh, 1975). Most commonly, this element is present as discrete Sn-bearing minerals in sulfide ores (e.g., at Neves Corvo, Portugal; Benzaazoua et al., 2003). Oen et al. (1980) indicated that sphalerite and stannite form a limited solid solution series. This led Shimizu and Shikazono (1985) to propose that element partitioning between coexisting stannite and sphalerite could be an indicator of temperature and sulfur fugacity. Ono et al. (2004) have documented 1.8–4.3 wt.% Sn in (In-bearing) sphalerite from the Suttsu deposit, Japan.

Confirmations of *arsenic*-bearing sphalerite are few, despite numerous claims of arsenian sphalerite before the pre-electron microprobe era. Clark (1970) summarized early data, determined concentrations of 1.7 ± 0.3 wt.% As in bright pink sphalerite from Alacran, Chile, and proposed low-temperature arsenian sphalerite solid solution Zn(As, S). More recently, As has been reported in sphalerite from black shale deposits (e.g., Orberger et al., 2003) at concentrations in the hundreds of ppm range.

Antimony is uncommonly reported in sphalerite. An unusual color-banded sphalerite from BC, Canada is described as containing Sb up to a maximum 0.55 wt.% Sb (Beaudoin, 2000). Kelley et al. (2004) reported 0.4–2400 ppm in yellow to reddish-brown sphalerite from Red Dog, Alaska. *Bismuth* does not appear to be enriched in natural sphalerite.

Cabri et al. (1985) report *selenium* concentrations from <mdl (43 ppm) to 292 ppm in 'C' zone ore from Kidd Creek ore. Orberger et al. (2003) provide PIXE data showing hundreds to thousands of ppm Se in sphalerite from black shale deposits in the Selwyn Basin. Pirri (2002) reports 0.12 wt.% Se in sphalerite from the Baccu Locci Mine, Sardinia, where most coexisting sulfides are Se-bearing. There exists a complete solid solution between sphalerite and stilleite (ZnSe). *Tellurium* is known to enter most sulfides at low concentrations, but there are few reports of significant Te concentrations in the modern literature. Huston et al. (1995) report Te concentrations in excess of mdl (>20–30 ppm) in only four grains. Limited solid ZnS–ZnTe solid solution is suggested by available phase diagrams (e.g., Tomashik et al., 1978).

3. SAMPLE MATERIAL

Concentrations of trace elements have been documented in sphalerite from 26 ore deposits (Table 2). The samples

Table 2
Deposits and sample location.

Deposit, sample	Type of ore sampled, location, conditions of formation	Sphalerite-bearing paragenesis	Mining history, tonnage, ore grade	Reference(s)
Epithermal-style deposits				
Neogene epithermal, Southeastern Europe Gold deposits in Golden Quadrilateral, S. Apuseni Mts., Romania				
Baia de Aries (BdA)	Base metal breccia pipe (Valea Lacului)	Py-Sp-Ga-Tet	Exploited until 2004	Ciobanu et al. (2004a) and references therein
Hanes (H-1962)	Au–Ag-(base metal) vein	Py-Sp-Cp-Ga-St	Exploited until mid-1990s	Ciobanu et al. (2004a) Cook and Ciobanu (2004)
Larga (L-82)	Au-(base metal) vein, "Geode area" Sp–St geothermometry: formed at >350 °C	Py-Sp-Cp-Ga-tel	Historical production; explored in 1980s	Cook and Ciobanu (2004)
Rosia Montana, Black breccia (CRC, RM-21)	Au-base metal vein within diatreme breccia deposit	Sp-Py-Tet-Argy-tel	Part of giant >215 Mt deposit (10.1 Moz Au, 47.7 Moz Ag)	Ciobanu et al. (2004a,b) and Tamas et al. (2006) http://www.gabrielresources.com
Magura (Mag-8)	Au–Ag-base metal vein	Py-Sp-Ga-Tet-tel	Exploited until 2005?	Ciobanu et al. (2004a)
Sacarimb (Sac 7.3, Sac 7.7)	Base metal sahlband of Au-telluride veins Fluid inclusion temperatures: 260–300 °C	Py-Sp-Ga-tel-ss	1.3 Moz Au produced up to 1989	Ciobanu et al. (2004a, 2008) Alderton et al. (1997)
East Carpathians				
Toroiaga (Tga-1)	Au–Ag-bearing base metal vein Estimated formed at 350–400 °C	Py-Sp-Ga-Tet-ss	Exploited until 2000	Cook (1997)
Late Cenozoic Magmatic Zone, Northern Japan				
Toyoha Zn–Pb–Cu–In (In-1, In-2)	In-bearing sphalerite vein (Izumo vein)	Sp-Asp-Py-Cas	Exploited 1914–2005. Production up to 1974: 7.547 Mt @ 121 g/t Ag, 3.0% Pb, 7.4% Zn (after 1974, Sn, In, etc. were mined at SW area)	Ohta (1989, 1991, 1995), Watanabe (1990), Watanabe and Ohta (1995)
Skarn deposits				
Late Cretaceous Banatitic Magmatic and Metallogenic Belt, Southeastern Europe				
Majdanpek, Serbia (MD20)	Zn-zone (associated with porphyry/epithermal Cu–Au)	Sp, hedenbergite skarn	Small reserve at periphery of main Cu–Au deposit	Ciobanu et al. (2002)
Ocna de Fier (Banat, Romania)	Fe–Cu–Zn–Pb skarn		Exploited until 1993, 13 Mt ore	Ciobanu and Cook (2004)[see Fig. 2 in this paper for sample locations]
Paulus (P43)	Zn-zone, distal (north), level 206	Sp-Mt-Ga-Hem	30–35% Fe, 0.5% Cu	
Paulus (3375)	Dissemination in hornfels adjacent to skarn, level 206	Sp-Ga-Hem		
Simon Iuda (3910b)	Zn-zone, proximal-central, level 460	Sp-Ga-Bustamite		
Gratianus (54G)	Zn-zone, proximal (south), below level 460	Sp-Hem		
Stefania (St1)	Fe-zone, proximal-marginal (south), open pit	Sp-Py-Ga		
Baita Bihor (N. Apuseni Mts., Romania)	Cu–Mo–Zn–Pb–Au–Ag–Bi skarn		Production currently ceased	Cioflica et al. (1977), Ciobanu et al. (2002)
Antoniu North (BB19CB)	Cu–(Zn–Pb) inner skarn, level 16 (325 m)	Bn-Cp-Sp-Ga, Wit, Roq, Co-mins	5 Mt (?), 0.56 Cu, 1.06, Zn, 0.46 Pb, 0.09 Mo	
Antoniu (BB16C)	Zn–Pb outer skarn, level 17 (278 m)	Sp-Bn sympectites, Cp, Wit		
Antoniu North (BB6)	Zn–Pb deeper skarn, level 18 (228 m)	Py-Sp-Ga-Bn-Cp		
Marta (BB23)	Carbonate-hosted Zn–Pb ore, Speranta adit (576 m)	Sp-Ga-Py		
Valea Seaca (VS 1b)	Sphalerite in pyritic ore	Py-Sp-Ga		

Table 2 (*continued*)

Deposit, sample	Type of ore sampled, location, conditions of formation	Sphalerite-bearing paragenesis	Mining history, tonnage, ore grade	Reference(s)
Baisoara (N. Apuseni Mts., Romania) Cacova Ierii (Bs7a/g)	Fe-skarn with smaller volumes of Zn–Pb ore Carbonate-hosted Zn–Pb ore, level 200 (405 m)	Sp-Ga	Production currently ceased 20 Mt Fe ore, Zn–Pb ore <1 Mt	Ciobanu et al. (2002)
Other skarn deposits				
Kamioka, Hida Metamorphic Belt, Japan (Kam-1)	Zn–Pb skarn	Sp-Ga-Py	Exploited 720(?) – 2003 Production (1941–1974): 28 Mt @ Au 6.0 ppm, Ag 6.1 ppm,Cu 0.5% Pb 1.2%, Zn 6.2%, pyrite 14.3%	Kunugiza (1999)
Konnerudkollen, Oslo Paleorift, Norway (Ko99-2)	Zn–Pb–(Ag) skarn Fluid inclusion temperatures in quartz ~280 °C 6.3 wt.% NaCl equiv.	Sp-Ga-Py-Cp-Ai	Exploited 1731–1913 (1700 t Zn, 600 t Pb, 36 t Cu, 6.9 t Ag)	Segalstad and Telstø (2002)
Lefevre, CLY, BC, Canada (L-12)	Zn ore associated with Au–Bi–Au skarn	Py-Sp-Ga-Po-Cp	Occurrence currently in exploration	Howard (2007)
Stratabound deposits				
Carbonate-replacement Zn–Pb deposits				
Tres Marias mine, Chihuahua, Mexico (TM)	Ge-rich sphalerite in low-temperature MVT-type ore	Sp-Ga	Production 1949–1992 135,000 t ore @ 20% Zn, 300 g/t Ge; 150,000 t sulfide ore reserves @ >20% Zn, 130–160 g/t Ge & 100,000 t oxide ore	Saini-Eidukat et al. (2009); http://www.wareaglemining.com
Sinkholmen, Svalbard (Znh1)	Carbonate-hosted sphalerite	Sp-Ga-Fl	Small occurrence, 240 t ore mined in 1920s	Flood (1969)
Kapp Mineral, Svalbard (KMi5)	Carbonate-hosted sphalerite	Sp-Ga	Small occurrence, exploration in 1920s	Flood (1969)
Melandsgruve, Hitra, Norway (Hit-1)	Pb–Zn, carbonate-replacement/skarn	Py-Cp-Sp-Tet-Ga	Small occurrence, mined in early 20th Century	Geol. Surv. Norway (www.ngu.no)
Volcanogenic massive sulfide deposits				
Vorta, S. Apuseni Mts., Romania (DMV)	Jurassic ophiolite-hosted VMS ore	Py-Sp-Ga-Tet-En	Exploited until recently, ~2 Mt (?)	Ciobanu et al. (2001)
Eskay Creek, BC, Canada (P5)	Polymetallic VMS ore, Bowser Basin (Jurassic)	Py-Sp-Ga-Tet-ss	Production – 2002: 2.25 Moz Au, 104.7 Moz Ag	Grammatikopoulos et al. (2006)
Sauda, Western Norway (Sa-1)	Massive sphalerite ore (Sveconorwegian)	Sp-Py-Cp-Ga	12,000 t ore mined (early 20th century) @ 32% Zn, ~1% Cu	Geol. Surv. Norway (www.ngu.no), Andersson et al. (2004)
Bergslagen District (Svecofennian, South-Central Sweden)				
Zinkgruvan (Zn99.1)	Massive sphalerite–galena ore	Sp-Ga	Production 1857-date, 34 Mt ore up to 2008 Reserves 10.8 Mt @ 9.4% Zn, 4.7% Zn, 102 g/t Ag	Hedström et al. (1989) http://www.lundinmi-ning.com
Kaveltorp (Kv99.1)	Cu–Zn–Pb massive sulfide/skarn	Cp-Sp-Ga-Py	Mining until 1970s	Grip (1978)
Marketorp (Ma99.4)	Zn–Pb–Cu massive sulfide	Py-Sp-Ga-Cp	Historical mining	Sundblad (1994)

Mineral abbreviations: Py – pyrite, Cp – chalcopyrite, Sp – sphalerite, Ga – galena, Tet – tetrahedite, Po – pyrrhotite, En – enargite, Fl – fluorite, St – stannite, Cas – cassiterite, Ai – aikinite, Argy – argyrodite, Bn – bornite, Wit – wittichenite, Co-mins: Cobalt-bearing minerals (carrollite, etc.), Roq – roquesite, tel-tellurides, ss – sulfosalts.

selected for study were biased towards suitable, coarse-grained and material generally free of visible inclusions, except for those carrying "chalcopyrite disease". The study purposely included a number of unusual sphalerites with exceptionally high concentrations of Mn, Cd and In (up to 5, 10 and 12 wt.%, respectively). Incorporation of

samples from the same deposit or metallogenetic province, e.g., 'Golden Quadrilateral', Romania (GQ; 6 deposits; Ciobanu et al., 2004a) and Late Cretaceous Banatitic Magmatic and Metallogenic Belt of Romania, Serbia and Bulgaria (BMMB; four deposits; Ciobanu et al., 2002), allows for identification of local and/or regional trends using minor/trace elements in sphalerite. A brief outline of the deposits is given below.

3.1. Epithermal deposits

Most of the deposits in the GQ are Au veins of epithermal, low-sulfidation, type; several are breccia-hosted (e.g., diatreme breccia at Rosia Montana, magmatic breccia at Baia de Aries). Sacarimb is a typical Au-telluride deposit. The samples from the latter are from the base metal mineralization in the sahlband of Au-telluride veins that typically contain significant amounts of Pb–Sb sulfosalts and Au(Ag) tellurides (in particular nagyágite). Similar features are present in the sphalerite from the veins at Magura, a deposit situated ca. 10 km to the WNW. In this case, besides sulfosalts and tellurides, inclusions of native gold are also abundant in sphalerite.

Characteristic for the GQ is that some of the veins are opened onto porphyry roots, e.g., Larga. The latter orefield, and others in the GQ (e.g., base metal orepipes at Baia de Aries, rhodochrosite–Ag–Au veins in the black breccia at Rosia Montana) also include skarn features. Secondly, in most of the deposits in the GQ, besides Au (Ag) there is also base metal mineralization present, either in intermediate to deeper parts of the same veins; e.g., Hanes, Larga), or as separate orepipes (Baia de Aries). At least some of the deposits (e.g., Larga; Cook and Ciobanu, 2004; Baia de Aries, Ciobanu et al., 2004a and references therein) are interpreted to have formed at higher-temperatures (>300 °C) than are typical for low-sulfidation epithermal deposits. The same is true for Toroiaga, Eastern Carpathians (Cook, 1997).

Indium-bearing deposits are abundant on the Japanese Islands, both within the Late Cretaceous–Paleogene Inner Zone of SW Japan and in Late Cenozoic Magmatic Zones of Central and Northern Japan (Ishihara et al., 2006). High-grade Zn–Pb pull-apart vein systems of the Pliocene (2.93–0.49 Ma) Toyoha deposit (Watanabe, 1990; Ohta, 1995), hosted within Miocene clastic and pyroclastic rocks and formed beneath a stratavolcano, contained a pre-mining resource of 4700 t In metal. Although the indium ores at Toyoha are perhaps the most famous, a dozen or more other localities are known, including Ikuno, Ashio, Kawazu and Akenobe (Ishihara et al., 2006). The unique geological environment offered by the collage of accreted terranes intruded by various deep oxidized magmas, and mixing of magnetite- and ilmenite-series belts, has been invoked to explain the In enrichment across Japan (Ishihara et al., 2006).

Indium enrichment at Toyoha relates to later-stage mineralization, with spectacular values only recorded in these veins, especially in the Sorachi and Izumo-Shinano veins in the SW part of deposit (Ohta, 1989, 1992). Although roquesite, sakuraiite and other discrete In-bearing minerals are observed, most indium is hosted within rhythmically-banded sphalerite. One of our specimens (In-1) comes from the high-grade bonanza ores (>1000 ppm In) of the E-W-striking Izumo vein along the '430 mL' level. Apart from the extremely In–Cu and Sn–Ag-rich sphalerite, the specimen is characterized by an abundance of zoned arsenopyrite and deficiency in Sn-minerals other than cassiterite.

3.2. Skarn deposits

All skarn deposits studied from the BMMB are zoned. Orefield zonation along a 10 km strike at *Ocna de Fier* (Fe–Cu/Fe/Zn–Pb) is centered upwards and laterally onto a fluid source in the median part of the deposit (Ciobanu and Cook, 2004). Samples were investigated from both the median Fe (Stefania) and upper/lateral Zn–Pb zone in the central (Simon Iuda, Gratianus) and distal orebodies (Paulus) (Table 2).

The skarn at *Baita Bihor* includes ~10 main orepipes that are structurally controlled by major faults. The contact with a magmatic intrusion is not exposed but a large granite body, lying some 1–1.2 km below the orebodies, and intersected in drillcores, is considered responsible for skarn formation. Although a lateral zonation, from W to E: Mo, Cu, Zn–Pb, can be considered based on the dominant type of ore, a local skarn zonation from core to outer margin of each orepipe (humite/pyroxene/garnet/wollastonite + carbonate), often with overlapping boundaries, is very prominent. The two orebodies sampled (Antoniu with a northern branch and Marta, some 1 km NNE from Antoniu) are from the Cu and Zn–Pb zones (Table 2). Sphalerite was investigated from (i) inner part of Antoniu North (spectacular bornite–sphalerite cm-size coarse exsolutions in diopside ± wollastonite skarn; BB19CB; level 16), (ii) andradite ± rhodonite + carbonate skarn in the outer part of Antoniu (BB16C; level 17), (iii) diopside skarn from the deepest part of Antoniu North (BB6; level 18) and (iv) carbonate-hosted sphalerite from Marta (BB23; Speranta mine). A smaller, vein-skarn deposit, Valea Seaca, historically exploited for Ag and Cu and situated 5 km to the NNE, is part of the same orefield; sphalerite was analyzed from a pyritic sample. Unlike other sphalerites from Baita Bihor, or any of the BMMB skarn samples analyzed here, displays marked chalcopyrite disease.

There are three Fe orebodies at *Baisoara* placed at direct contacts to magmatic apophyses. Unlike the two examples above, Zn–Pb ore (samples Bs7a, 7g) is known only from a small area placed within carbonate, several tens of meters outside the skarn contact (Cacova Ierii). The orefield also includes a small body of Zn–Pb ore in pyroxene–garnet–epidote skarn (Valea Lita) 3 km N of the Fe bodies.

The vein Zn–Pb skarn at *Majdanpek*, Serbia is situated ~1 km N from the giant epithermal/porphyry Cu mineralization in the same orefield. The sample analyzed here consists of monomineralic, rich Fe-sphalerite without chalcopyrite disease, which is typical for the hedenbergite skarn in the deeper part in the deposit. Carbonate-hosted Zn–Pb ore (sphalerite with chalcopyrite disease, galena, pyrite) occurs at upper levels (some 400 m above) and displays concentric/coccade textures.

Single samples from the following skarn deposits were also included: massive sphalerite in pyroxene skarn from the Zn–Pb zone, *Kamioka*, Japan (Cretaceous, Hida Metamorphic Belt); sphalerite in base metal ore from the Zn–Pb–(Ag) skarn at *Konnerudkollen* (Paleozoic Oslo Rift, Norway) and sphalerite–galena in the *Lefevre* Au–Bi–W skarn where a small Zn–Pb mineralization occurs towards the limestone contact. This is part of the CLY intrusion-related Au–Bi prospect (Paleozoic Kootenay Arc, SE BC, Canada).

3.3. Stratabound deposits

Specimens from 10 localities have been investigated (Table 2). The *Tres Marias* deposit, Chihuahua, Mexico has been interpreted as a Mississippi Valley type deposit (Saini-Eidukat et al., 2009). The orebody (29°08′34″N, 103°39′57″W) occurs in a mid-Cretaceous carbonate sequence, in a carbonate solution collapse breccia, the known extent of which reaches approximately 100 m below surface. Two major ore types exist: one consisting primarily of zinc and lead sulfides, and a sulfide-poor type (“oxidized ore”) of Zn-silicates, carbonates plus oxide minerals. The *Melandsguve* deposit, Hitra, is hosted by a Paleozoic sequence and has been included here, even if the deposit may have been formed at higher-temperatures, considering the skarn-like features (e.g., presence of pyroxene). The small Devonian (?) *Sinkholmen* and *Kapp Mineral* occurrences, Spitsbergen, are best interpreted as carbonate-replacement deposits, based on field relationships.

Among the VMS deposits, the Svecofennian Bergslagen Province, South-central Sweden, is represented by three examples, of which *Zinkgruvan* is a massive Zn–Pb–(Ag) ore, whereas *Kaveltorp* and *Marketorp* are Cu-rich, with some skarn-like features. The Sveconorwegian *Sauda* deposit, Norway, is also a massive Zn ore, in which certain parts of the ore have the character (e.g., presence of Cu–In–Sn–Bi–Se minerals; Andersson et al., 2004) of a syn-metamorphic remobilizate (see Marshall and Gilligan, 1987).

The deposit at *Vorta* is the largest VMS deposit in the Jurassic ophiolite sequence in the S. Apuseni Mts., Romania. Several Mo-deposits (granite-hosted veins) are known from the lower part of the same sequence to the west. The origin of the Vorta deposit has been debated due to the presence of sulfide disseminations resembling porphyry-Cu style mineralization in restricted parts of the ore-field. The latter has been interpreted as relating to a presumed Late Cretaceous (?) magmatism (dacitic subvolcanic bodies) found elsewhere in S. Apuseni Mts. (Ciobanu et al., 2004a and references therein). The Vorta ore is typified by framboidal textures. Besides widespread tetrahedrite–tennantite and frequent inclusions of native gold, the ore also includes minerals indicative of a high-sulfidation environment, such as enargite.

The giant *Eskay Creek* polymetallic VMS deposit, Bowser Basin, NW BC, Canada, is hosted in a Middle Jurassic volcano-sedimentary sequence and is characterized by Au- and Ag-enrichment. The sphalerite sample analyzed is a Hg–Fe-rich specimen (average formula $Zn_{0.89–0.98}Hg_{0.01–0.09}Fe_{0.005–0.02})S$; Grammatikopoulos et al., 2006). The ore contains abundant tetrahedrite–tennantite and Cu–Pb–Sb–(As) sulfosalts.

3.4. Patterns and textures

One-inch polished mounts were prepared from each sample. Scanning electron microscopy in back-scattered electron mode was used to characterize each, paying particular attention to inhomogeneities within the sphalerite, mineral inclusions, compositional zoning, or other textural aspects, all of which may impact upon trace element distributions. Each specimen was also studied by electron microprobe to ascertain the Zn content, which would be used as the internal standard, and in some cases, to determine contents of minor elements (Fe, Mn, Cd, etc.) for comparison with the LA-ICPMS data.

Compositional zoning in sphalerite was readily recognized in several specimens, notably in those with ‘extreme’ concentrations of minor elements. Cadmium-rich sphalerite from the skarn at Baisoara (up to 11 wt.% Cd; sample Bs7) features oscillatory zoning with high-Cd cores (Fig. 1a), as well as sectorial zoning and rhythmic banding across precipitation fronts (Fig. 1b). This type of sphalerite typifies a carbonate-hosted ore that contains cavities coated by concentric, coccade textures with marcasite, pyrite, and galena as well as sphalerite.

Black breccia-hosted veins at Rosia Montana (GQ) are typified by Mn-bearing minerals, including rhodochrosite and pyroxmangite (Ciobanu et al., 2004b), as well as sphalerite with Mn-rich lamellae (sample RM-21; Fig. 1c). Nucleation of galena along the lamellae boundary is followed by replacement across the banding (Fig. 1d).

Samples from Hanes and Baia de Aries (GQ) display spectacular ‘chalcopyrite disease’ including a fine-scaled mottling that is suggestive of incipient chalcopyrite disease. Some of these are suggestive of chalcopyrite grain size variation from micron- to nano-scale in the cores of the grains; sample BdA, Fig. 1e).

The specimen from Tres Marias consists of Ge-rich sphalerite with a bladed habit as indicated by the patterns observed on back-scattered electron images (Fig. 1f). Variation in gray shades indicates variable Fe content; this corresponds to the Type I sphalerite of Saini-Eidukat et al. (2009). Such patterns are further complicated by a series of irregular to lamellar ‘grate’-like features within each blade. A ragged replacement front within the bladed sphalerite is marked by increased porosity occurring along the described pattern. This replacement has led to a decrease in the Fe content of the sphalerite from 8–9 wt.% to 2–4 wt.%.

Both In-bearing specimens from the Toyoha veins, Japan, display rhythmic patterns as: (i) mm-scale rhythmic banding between sphalerite (reddish color) and fine-grained Cu–Pb–Fe–As-sulfide ore (dark gray-black) (In-2) and (ii) mineral banding and microscopic-scale oscillatory/sectorial zoning (In-1). Characteristic for both samples is the presence of arsenopyrite within and adjacent to sphalerite that displays patterning (Fig. 2a and b). The Fe content in sphalerite is comparable in the two samples (~4.5–6 wt.%).

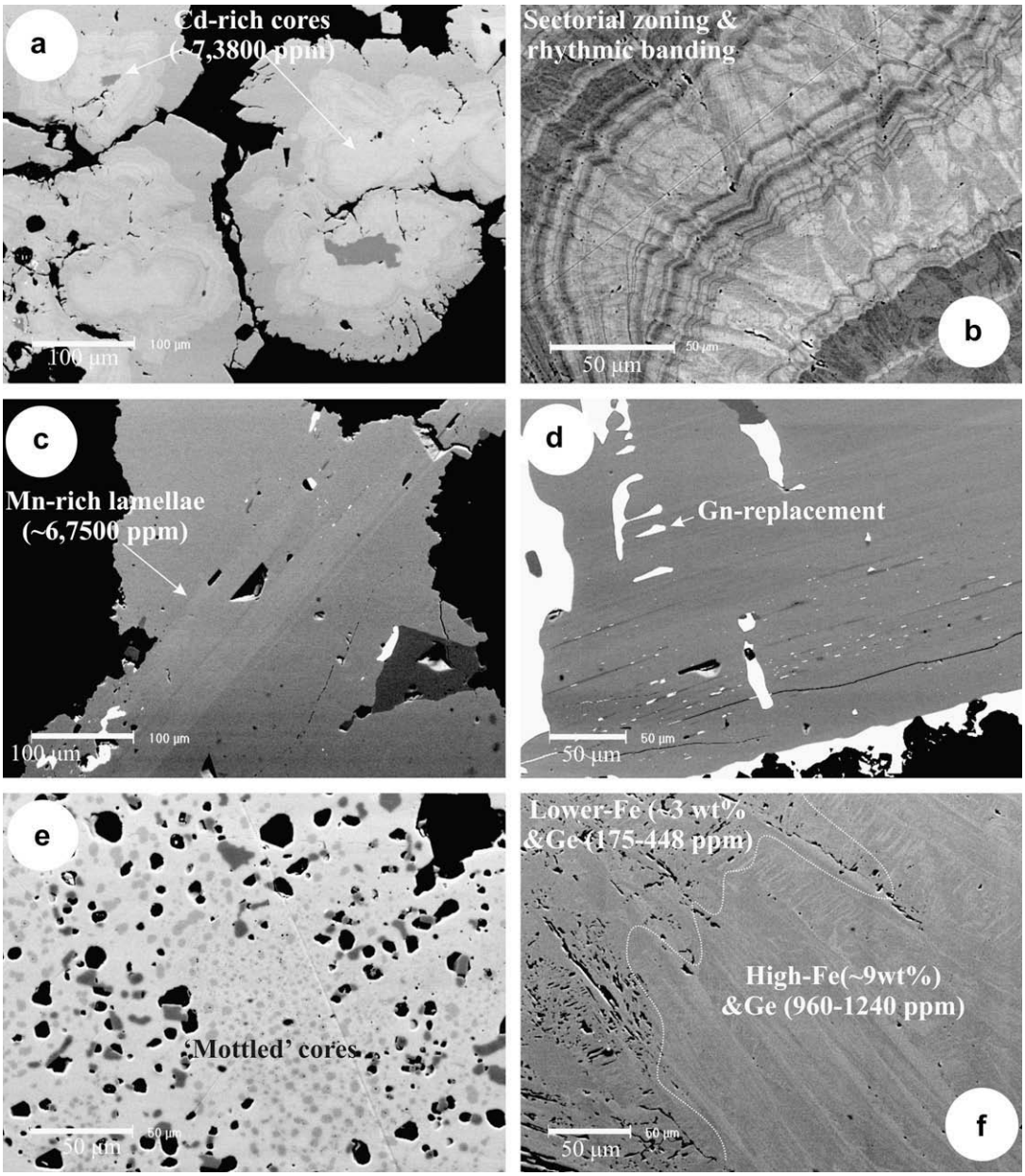

Fig. 1. Back-scattered electron images illustrating patterns in sphalerite. (a) Oscillatory zoning and banding in Cd-bearing sphalerite and (b) Detail of sectorial zoning and rhythmic banding in sphalerite crystal Cp: chalcopyrite (Baisoara; Bs7a). (c) Manganese-rich lamellae in sphalerite and (d) replacement of sphalerite by galena along and across the lamellae (Rosia Montana; RM-21). (e) "Chalcopyrite disease" as mottled cores in sphalerite (Baia de Aries; BdA). (f) Patterns showing bladed habit in sphalerite and with irregular to lamellar 'grate'-like features within each blade. A ragged replacement front within the bladed sphalerite is marked by increased porosity occurring along the described pattern. Note the compositional difference across the replacement front (Tres Marias; TM).

In sample In-2, besides the macroscopic pattern described above, there is a finer banding within the sphalerite itself (tens of μm) realized by differences in porosity. In the less porous sphalerite the banding is also outlined by oscillatory zonation patterns in crystals growing along and towards the inner parts of the bands (Fig. 2a); coarser grains of arsenopyrite, also with oscillatory zonation, are abundant in such bands. In the darker bands the sulfide ore comprises a mixture of finely intergrown pyrite, chalcopyrite, galena and arsenopyrite is various proportions.

Sample In-1 consists of coarse-grained sphalerite interspersed with up to cm-size arsenopyrite and pyrite. Patterning is observed throughout the entire mass of sphalerite, but the oscillatory zonation comprising zones with high- and low-In is superimposed onto a pre-existing low-In and high-Fe pattern and is also tied to the occurrence of arsenopyrite (Fig. 2b). Irregular, highly porous areas, as in sample In-2, are present within the high- and low-In zonation. The bands within these patterns can reach up to 1 mm in width, but individual grains are commonly zoned across several

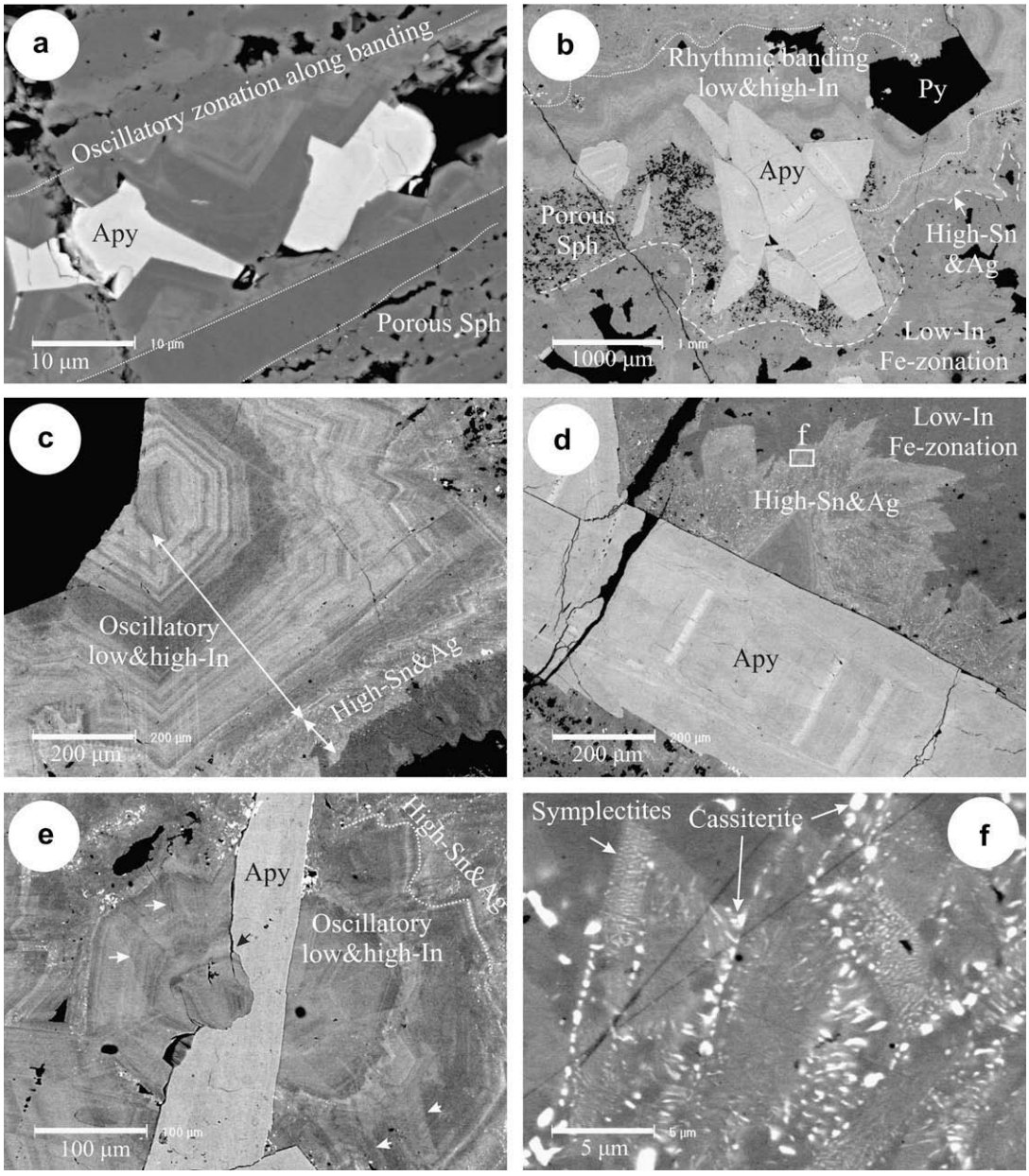

Fig. 2. Back-scattered electron images illustrating patterns and textural aspects in sphalerite from Toyoha (all In-1 except (a)). (a) Banding realized by differences in porosity; note oscillatory zonation in crystals growing along and towards the inner parts of the bands. (b) Oscillatory zonation/banding comprising zones of high- and low-In (dotted line) with outer high-Sn–Ag margin (dashed line), both superimposed onto pre-existing low-In and high-Fe pattern; note the porosity in sphalerite and the presence of arsenopyrite (Apy) within such zones. (c) Detail of single crystal oscillatory high and low-In zonation with an outer high-Sn–Ag margin. (d) Sn–Ag-rich zone in sphalerite growing outwards from the margin of a zoned arsenopyrite (the arsenopyrite contains 0.7–10 ppm Au; authors LA-ICPMS data). Note fractures and porosity. Small rectangle indicates location of detail in (f). (e) Corrosion of arsenopyrite by high- and low-In-zoned sphalerite. Note sectorial zoning marked by white arrows. (f) Symplectites of Sn–Ag-bearing phases and Sn–Ag-rich sphalerite. Note nucleation of cassiterite.

hundreds of µm (Fig. 2c). The zonation displays several recurrent cycles but the outer margin of the pattern is high in Sn and Ag (Fig. 2c, d). Arsenopyrite, also zoned, is cross-cut by fractures (Fig. 2d) and corroded by high- and low-In-sphalerite (Fig. 2e). In the latter case, the zonation in sphalerite is underlined by grains of cassiterite and/or other Sn, Ag-bearing phases. In detail, the high-Sn and Ag zones feature fine symplectites between sphalerite and Sn-(Ag)-bearing phases (Fig. 2f).

4. EXPERIMENTAL

LA-ICPMS analysis of sphalerite was made using the Agilent HP4500 Quadripole ICPMS instrument at CODES

(University of Tasmania, Hobart, Australia). This instrument is equipped with a high-performance New Wave UP-213 Nd:YAG Q-switched laser-ablation system equipped with MeoLaser 213 software. The laser microprobe was equipped with an in-house small volume (~2.5 cm^3) ablation cell characterized by <1 s response time and <2 s wash-out time. Ablation was performed in an atmosphere of pure He (0.7 l/min). The He gas carrying the ablated aerosol was mixed with Ar (1.23 l/min) immediately after the ablation cell and the mix is passed through a pulse homogenizing device prior to direct introduction into the torch.

The ICPMS was optimized daily to maximize sensitivity on mid- to high-mass isotopes (in the range 130–240 a.m.u.). Production of molecular oxide species (i.e., $^{232}Th^{16}O/^{232}Th$) and doubly-charges ion species (i.e., $^{140}Ce^{++}/^{140}Ce^{+}$) was maintained at <0.2%. Due to the low level of molecular oxide and doubly charged ion production, no correction was introduced to the analyte signal intensities for such potential interfering species. Each analysis was performed in the time-resolved mode, which involves sequential peak hopping through the mass spectrum.

The laser system was operated at constant 5 or 10 Hz pulse rate; laser energy was typically 5–6 J cm^{-2}. At these conditions each pulse removes ~0.3 μm of the samples, resulting in ablation rates of 1.5 μm/s and 3.0 μm/s for 5 and 10 Hz, respectively.

Pre-defined areas of the polished blocks were ablated; spot sizes of the 319 analyses varied from 25 to 80 μm in diameter. The following isotopes were monitored: ^{55}Mn, ^{57}Fe, ^{59}Co, ^{60}Ni, ^{65}Cu, ^{66}Zn, ^{69}Ga, ^{72}Ge, ^{75}As, ^{77}Se, ^{95}Mo, ^{107}Ag, ^{111}Cd, ^{115}In, ^{118}Sn, ^{121}Sb, ^{125}Te, ^{197}Au, ^{202}Hg, ^{205}Tl, ^{208}Pb and ^{209}Bi. The analysis time for each sample was 90 s, comprising a 30-s measurement of background (laser off) and a 70-s analysis with laser-on. Acquisition time for all masses was set to 0.02 s, with a total sweep time of ~0.6 s. Data reduction was undertaken according to standard methods (Longerich et al., 1996) using Zn as the internal standard.

Calibration was performed using an in-house standard (STDGL2b-2), comprising powdered sulfides doped with certified element solutions and fused to a lithium borate glass disk. This standard is suitable for quantitative analyses in different sulfide matrixes (Danyushevsky et al., 2003, in press).

A series of correction factors (Danyushevsky et al., in press) were applied to the measured ppm values in each analysis as follows: Mn 1.46, Fe 1.49, Co 1.51, Ni 1.59, Cu 1.53, Ga 1.45, As 1.36, Se 1.85, Mo1.62, Ag 1.40, Cd 1.50, In 1.45, Sn 1.6, Sb 1.17, Te 1.00, Au 1.40, Tl 2.17, Pb 1.37, Bi 1.33. These correction factors were established by analyzing sphalerite secondary standards using STDGL2b-2 and reflect significant elemental fractionation between Zn in most other elements during laser-ablation. The error on the correction factors is <5% as determined by comparing the correction factor derived using different laser systems (213 nm and 193 nm). Analytical accuracy is expected to be better than 20% with variations in spot size being the main additional contributing factor.

Concentrations of germanium cannot be quantified with full confidence because the isotope weight of 72 is equal to $^{40}Ar^{32}S$ (and also $^{40}Ar^{32}O$ in the standard), and the Ge concentration in the standard is not high enough to ignore these interferences. For this reason, there is uncertainty concerning exactly how much Ge is in the standard and no Ge value is published for STDGL2b-2 (Danyushevsky et al., in press). Higher germanium values (>20–30 ppm) may, however, be confidently compared with one another. Quantification of Hg is not possible as these elements are not present in the calibration standard. Relative variations in the concentrations of both Ge and Hg can be assessed by comparing the observed count intensities normalized to those of the internal standard in each analysis.

The raw analytical data for each spot analysis was plotted as a line graph and the integration times for background and sample signal selected. The counts are then corrected for instrument drift (standards were run each 2 h) and converted to concentration values using known values of a major element in the analyzed minerals as an internal standard.

Based on the measured concentrations, detection limits were calculated for each element of interest (Electronic Appendix). These values depended on the spot size, which influences the volume of ablated mineral and thus the count rates for each spot. The error on the element signal is calculated as $(\sigma/\sqrt{n}) \times 100$, where σ is the standard deviation and n the number of data points across the selected signal interval. Total analytical error (precision) is expressed as a percentage of concentration and is an expression of analytical noise. The smooth profile, and good precision, observed for almost all analyses indicates the specimens to be homogeneous. In the subsequent section, mean analyses for a given element in sphalerite from a specific deposit is referred to. These are simple numerical means of n individual analyses.

We had intended to offer compositional data for As for the full dataset, but high background counts on one of our analytical runs made this impossible.

5. RESULTS OF LA-ICPMS ANALYSIS

The LA-ICPMS dataset (319 spot analyses; Electronic Appendix) shows concentrations of each minor/trace element in natural sphalerite to typically range over several orders of magnitude. An important exception to this is Cd, which appears at fractions of percent in all samples, except in sample Bs7a, where concentrations reach wt.% levels and closely match those determined by EPMA (difference in mean analyses, 4% relative). Despite our efforts to analyze sphalerite volumes free of obvious inclusions or other features, the analyzed samples (Figs. 1 and 2) do nevertheless show extensive inhomogeneity, at least in some samples. Since the LA-ICPMS spot size is greater than many of these features, it is reasonable to expect that the ablation profiles will not always show homogeneity on the scale of the ablation spot. The ablation profiles for some elements (In, Mn, Cd, Ge, Ga, Co, etc.) are smooth, suggesting that these are homogenously distributed on the scale of the spot. Other elements, notably Pb, Bi, and in some samples, also Ag

and Tl, commonly – though not always – display irregular profiles suggesting the presence of micro-scale inclusions of minerals carrying those elements. Mean concentration data are summarized in Table 3, with those data suggesting inhomogeneous distributions indicated (as standard deviation>mean concentration). Concerning the size of inclusions that will be identifiable on the spectrum, some approximate estimations may be given, even if quantification is difficult. If the concentration of a given trace element in sphalerite is 10,000 less than in the inclusions, then an inclusion 100 times smaller than the spot size will be identifiable. If the concentration in sphalerite is 1,000,000 less than in the inclusions, then an inclusion 1000 times smaller than the spot size will be identifiable. Mean minimum detection limits (mdl), standard deviations, maxima, minima, mean precisions (%) and mean stage error (%) are given in the Electronic Appendix. Representative single-spot spectra, showing both smooth and irregular profiles, selected from the complete dataset are shown in Figs. 3–5.

Individual samples are rich in specific elements (Table 3). A number of general rules regarding absolute abundances and inter-element correlations are recognized, which will be reported in the following sections, firstly by deposit type, and in specific deposits (Sections 5.1–5.3), and then in terms of elements (Section 5.4).

5.1. Epithermal deposits

Element concentrations in sphalerite in samples Tg-1 from Neogene vein-mineralization in Romania at *Toroiaga*, L-82 from *Larga* and H-1963 from *Hanes* show similarities. All three cases have been regarded, on the basis of coexisting assemblages (Cook, 1997), and the presence of *iss* in the case of Hanes (Cook and Ciobanu, 2004), as representing higher-temperatures (>300 °C). Sphalerite from all three occurrences contain significant In contents, with L-82 particularly enriched (mean 669 ppm). In all cases, In displays a strong correlation with Cu. Tin enrichment in sphalerite from sample L-82 (Fig. 3a), appears to be in solid solution, but is consistent with observed exsolution of stannite elsewhere in the sample, but never within sphalerite. Sphalerite from sample BdA-1 from a Zn–Pb breccia pipe at *Baia de Aries* in another district from GQ (Ciobanu et al., 2004a), also displays significant In enrichment (mean 141 ppm). The mottled chalcopyrite disease (Fig. 2e) is reflected in the series of peaks displayed by the Cu signal (Fig. 3b). Peculiar for some of the deposits in the GQ is the pronounced enrichment in Mn, e.g., Baia de Aries, Sacarimb, Rosia Montana and Magura; in the first two, alabandite is also abundant in the polymetallic ores.

Sphalerite from two deposits in another district in the GQ shows no In enrichment in sphalerite, i.e., sample Mag-8 from *Magura*, and the two samples from *Sacarimb* (Fig. 3c). Instead, they show significant enrichment in Ga and Ge, and in the case of *Magura*, also in As; both these deposits are considered within temperature ranges of epithermal deposits (lower than Hanes and Larga). The LA-ICPMS spectra for Sacarimb (Fig. 3c) shows characteristically ragged signals for many trace elements (Pb, Sb, Ag, etc.), indicating the presence of submicro- and nanoscopic inclusions of sulfosalts. Seven of the eight spot analyses from Magura have gold values between 2.7 and 17.9 ppm. Although the gold signal is irregular, and commonly correlates with components of sulfosalts (Cu, Pb, Ag and Sb), one spectrum (Fig. 3d) shows a smooth Au signal parallel with Te (16–665 ppm) and also As. A similar trend of Ga and Ge enrichment and low-In is seen in sphalerite from black breccia veins crosscutting the giant *Rosia Montana* diatreme breccia deposit; one sample (CRC-7) containing mean values of 366 ppm Ga, appreciable Ge (Fig. 4a), and also smooth signals for Sn. This mineralization hosts the discrete Ge-bearing mineral argyrodite (Ciobanu et al., 2004b; Tamas et al., 2006). Alabandite from Sacarimb (Fig. 4b), whether Fe-poor without coexisting sphalerite (sample Sac 7.4), or Fe-rich coexisting with sphalerite (Sac 7.7), is markedly enriched in As, Ag, Sb and Mo, and poor in Cd relative to sphalerite in the deposit (Table 3).

Sphalerite in sample In-1 (Toyoha) shows some of the clearest correlations between spectra and zonation patterns. For this sample, the dataset has been separated into those with lower-In, high-In and high-Sn (Table 3). In the In-rich bands, the high In concentrations correlate with increased Cu and Ag. The bands richer in Sn (Fig. 4c) also contain elevated In and Cu, but are still richer in Ag compared to the In-rich bands, with a good correlation between Sn and Ag. Sphalerite in this sample is generally rich in Ga, although lower in the In- and Sn-rich bands, but is relatively poor in most other trace elements, even if elements such as Pb, Sb and Bi display smooth signals on the spectra. These characteristics are also valid for the second sample from Tohoya (In-2), albeit with lower In concentrations (mean 2070 ppm).

5.2. Skarns

The sample from *Majdanpek* also shows rather flat profiles for most elements. The high-Fe-sphalerite also contains significant Mn, fairly low Cd, moderate Cu (some variance) and notable concentrations of In (tens of ppm), without any correlation with Cu. Silver, Pb and Bi are low.

Distal Zn skarn from *Ocna de Fier* (sample P43) shows flat profiles for most elements. Most analyses were of low-Fe-sphalerite, hosted in carbonate, even if sphalerite hosted by hedenbergite skarn in Paulus is typically Fe-rich (~20 mol.% FeS). All profiles show a wide range of Cu, Pb, Bi concentrations. Highest values correlate with enhanced Ag, Se and Te, which also show ragged profiles. These patterns can be readily attributed to micro- and nano-scale inclusions of sulfosalts, tellurides and selenides known from the deposit (e.g., Ciobanu and Cook, 2000; Cook and Ciobanu, 2001, 2003b). There is marked variation in Co values that appears lowest in the Fe zone (mean 25, Stefania) and highest in the Zn zone (mean 570 ppm, Gratianus); the first sample is the richest in Fe (6.6–7.8 wt.%) in the dataset. Data for three other samples from the same deposit (3910b, 54G and 3375; see Table 3) further emphasize the variable ranges of concentration in a single deposit. Sphalerite in sample 3375 (hornfels in Paulus) contains an average of 2300 ppm Co, the highest in our dataset, and, to

Table 3
Mean concentrations for minor and trace elements in sphalerite, and of alabandite in two specimens from Sacarimb. Data are in ppm (except Fe).

Sample	Ag	As	Bi	Cd	Co	Cu	Fe (%)	Ga	Ge[#]	In	Mn	Mo	Ni	Pb	Sb	Se	Sn	Tl
Epithermal deposits																		
Neogene epithermal mineralization (SE Europe)																		
Baia de Aries BdA (6)	3	–	0.2	4653	<mdl	1353	4.38	3.2	0.9	141	8040	0.2	0.1	0.7	0.1	4.5	4	0.3
Hanes H-1962 (8)	12	–	7*	4052	8	719*	8.96	3	1	46	4532	<mdl	<mdl	7*	1	11	54	<mdl
Larga L-82 (8)	9	–	<mdl	5560	100	1088	10.44	5	1	669	874	<mdl	<mdl	1	<mdl	248	333	<mdl
Rosia Montana CRC-7 (10)	8	–	<mdl	2707	<mdl	754	1.27	366	73	38	44516	3	<mdl	6*	3	9	47	<mdl
Rosia Montana RM-21 (10)	7	–	<mdl	3502	1	1906	0.34	95	6	9	67573	2	<mdl	343*	<1	8	17	<mdl
Magura Mag-8 (8)[a]	102*	223	5	4463	<mdl	1261	0.06	61	58	1	24400	1	<mdl	5981*	761*	46*	10	1
Sacarimb Sac 7.3 (6)	15	–	<mdl	2594	<mdl	566*	0.44	53	4	1.5	2548	1	<mdl	28*	23*	12*	4	<mdl
Sacarimb Sac 7.7 (5)	205*	–	157*	3652	<mdl	906*	0.06	359	81	63	45704	2	<mdl	12150*	351*	770*	110	36*
Toroiaga Tga-1 (6)	7	–	<mdl	7751	1	1644*	7.16	4	1	93	763	<mdl	<mdl	<mdl	<mdl	4	<mdl	<mdl
Toyoha Cu–Zn–In deposit, Japan																		
In-1 low-In (3)	698	<mdl	6	8339	12*	2368	5.05	273	2	509	220	<mdl	<mdl	155*	109	5	1384	<mdl
In-1 high-In (7)	3102	<mdl	42*	8785	17*	36228	5.69	144	1	58752	71	<mdl	<mdl	104	10*	19*	1486	<mdl
In-1 high-Sn (8)	12054	<mdl	644*	9582	6*	24053	4.81	103	1	9660	118	<mdl	1	1064*	35	31	11703	<mdl
In-2 (4)	1400*	3	0.5	4507	38	2615*	4.49	191	4	2070	207	1	4	3731*	2010*	9	598	5
Skarn deposits																		
Late Cretaceous skarns (SE Europe)																		
Majdanpek MD-20 (8)	1.8	–	0.5	2898	34	251	9.04	0.6	0.8	56	3919	0.13	0.6	0.5	0.1	76	0.4	<mdl
Ocna de Fier																		
OdF P43 low-Fe (9)	15	–	31*	6227	151	181	1.77	0.2	0.6	0.1	2618	0.1	0.4	3240*	0.2	3	0.05	<mdl
OdF 3375 (6)	68*	0.3	140*	6763	2299	15	0.60	0.7	0.8	1.9	6758	0.4	0.6	12230*	0.1	10	0.1	0.18
OdF 3910b (8)	6.8	2.6	13*	5088	302	268*	3.01	0.4	1.1	17	6042	0.2	2.3	1539*	0.7	4.4	0.2	0.04
OdF 54G (6)	5.6	0.7	23*	5404	570	3785	1.96	0.2	1.1	17	2725	0.3	0.5	753	0.3	7.9	0.1	0.08
OdF St1 (6)	4.3	0.3	1.0	5845	25	486*	6.04	1.7	1.6	86	4627	0.3	0.6	332*	1.1	4.3	1.6	0.04
Baita Bihor (and Valea Seaca)																		
BB19CB (6)	20	–	1	5769	1183	2893	0.13	0.3	0.6	812	967	0.03	7.4	12	<mdl	20	0.4	<mdl
BB16C (6)	1.4	–	0.08	7838	504	53	1.29	1.5	0.6	24	3359	0.11	6.2	1.7	0.3	8	0.04	<mdl
BB6 (8)	8.5*	0.3	5.3	7352	599	244	1.30	1.0	1.1	223	3827	0.1	11.4	46*	0.5	7.5	5.4	0.03
BB23 (10)	4	–	<mdl	2262	29	31	0.80	4	1	29	970	<mdl	<mdl	<mdl	<mdl	120	<mdl	<mdl
VS 1b (6)	18	0.2	18*	5451	8	13122	2.86	2.8	1.3	60	1643	0.1	0.3	594*	0.3	3.7	21	0.02
Baisoara																		
Bs7a (11)	46	–	25	73800	9	1588	0.28	8	1	22	298	2	<mdl	436	25	6	33	13
Bs7g (10)	107*	2.2	5*	8656	13	978*	1.36	22	10	1	668	<mdl	1	4100*	313*	4	7	39

Other skarn deposits																		
Kamioka Kam-1 (8)	14*	–	303*	5446	230	3	2.04	0.1	0.6	1	1380	<mdl	3.2	1345*	<mdl	61	0.2	0.1
Lefevre (CLY) L-12 (8)	3.4	0.3	2.4	10804	328	306	10.4	0.8	2.3	180	3050	0.2	4.6	3.8	0.1	16	0.1	0.1
Konnerudkollen Ko99.2 (5)	93	0.4	171	2449	1547	389	0.43	0.5	0.7	7.6	545	<mdl	5.1	3451	<mdl	24	0.1	0.3
Stratabound deposits																		
Low-temperature carbonate-replacement deposits																		
Tres Marias Zn–Ge deposit, Mexico																		
TM low-Fe (10)	2.2	434	0.7	4720	0.2	7.5	3.14	24	252	0.1	8.5	3.4	0.9	3090	62	2.1	2.1	53
TM-high-Fe (12)	4.6	572	0.2	5434	0.4	29	8.72	2.6	1081	0.2	44	0.4	0.3	1349	11	1.7	3.9	158
Other deposits																		
Sinkholmen Znh1 (8)	37	28	0.3	3916	0.1	1452	0.3	82	4.6	0.5	2.3	0.1	<mdl	15	24	15	3.8	<mdl
Kapp Mineral KMi5 (10)	123	2.4	0.3	1011	8.6	814	1.74	16	13	2.1	101	<mdl	3.6	1354	33	2.5	16	<mdl
Hitra Hit-1 (8)	27	17	0.1	6938	15	344	1.58	2.7	1.0	0.2	108	<mdl	8	160	102	1.0	0.8	<mdl
Volcanogenic massive sulfides																		
Vorta DMV (8)	6	–	0.3	4744	<mdl	382	0.19	96	7	<mdl	530	58	<mdl	462*	3.2	1.1	<mdl	0.2
Eskay Creek P5 (12)	535*	211*	0.04	3852	0.04	770*	0.49	148*	2.1	1.4*	3265	3.1*	0.8*	11521*	20420*	1.3	13	3.6*
Sauda Sa-1 (10)	4	–	<mdl	2262	29	31	8.02	4	1.0	29	870	<mdl	<mdl	<mdl	<mdl	119	<mdl	<mdl
Zinkgruvan Zn99.2 (5)	6.5	0.1	0.1	3812	160	3.4	3.23	2.2	1.1	0.3	513	<mdl	0.7	43	1.2	0.1	0.1	<mdl
Kaveltorp Kv99.1 (7)	5.5	0.3	1.0	1660	11	1229	9,86	2.1	2.1	4.6	30032	0.9	1.0	1503	0.2	1.9	0.6	0.1
Marketorp Ma99.4 (8)	14	0.2	23	3250	170	4021	9.69	2.3	3.5	26	4104	0.1	0.2	12	<mdl	33	0.3	<mdl

Trace element compositions of alabandite in the Sacarimb specimens (coexisting with sphalerite in Sac 7.7)

							Fe ppm				Zn							
Sacarimb Sac 7.4 (5)	740	4173	1.3	55	<mdl	610	407	<mdl	1.5	0.2	54	28	<mdl	27	1049	7.3	0.5	1.1
Sacarimb Sac 7.7 (4)	941	6974	26	208	0.7	2027	54916	0.2	1.6	2.3	46	27	1.2	18	508	54	20	3.1

Ge[#] Absolute concentrations (in ppm terms) must be considered as approximate only due to uncertainties in Ge content of standard. See Section 4. Numbers are retained in the table for purposes of comparison between samples only.

Mean EPMA data for Cd (wt.%): H-1962 0.38, BdA 0.44; CRC-7 0.25, RM-21 0.33, Sa-1 0.19. Mean EPMA data for Mn (wt.%): H-1962 0.53, BdA 1.03; CRC-7 5.02, RM-21 6.50, Sa-1 0.11. Mean EPMA data for Fe (wt.%): H-1962 9.10, BdA 1.03; CRC-7 1.22, RM-21 0.34, Sa-1 7.79.

Mean minimum detection limits, standard deviations, maxima, minima, mean precisions (%) and mean stage error (%) are given in Electronic Appendix.

[a] Au ranges from 2.7 to 17.9 pm, Te from 16 to 665 ppm (see Electronic Appendix).

* Standard deviation > mean concentration value; – not analyzed (background too high).

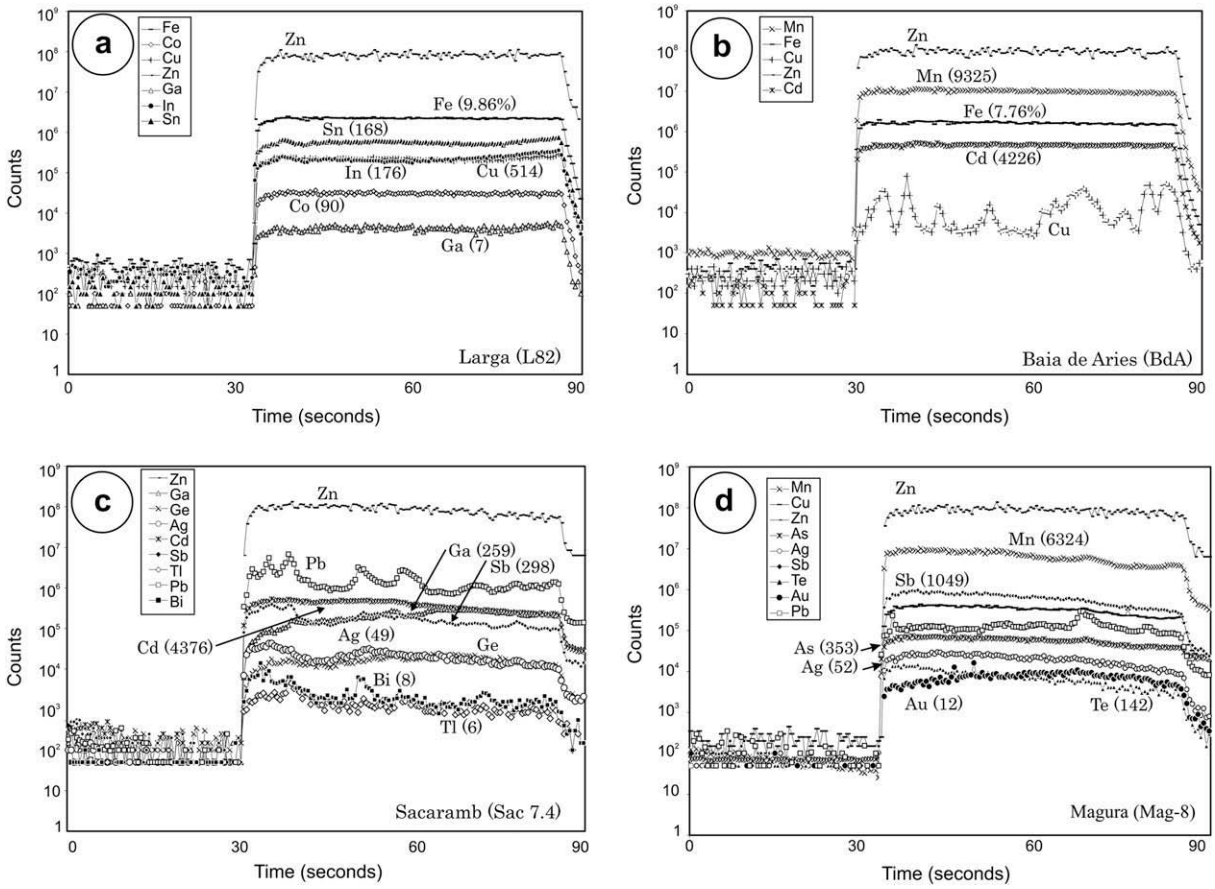

Fig. 3. Representative single-spot LA-ICPMS spectra for selected elements in sphalerite. Numbers in brackets are concentrations (in ppm). (a) Larga (L-82). Note smooth and parallel signals for all elements shown. (b) Baia de Aries (BdA). Note the series of ragged, small peaks with comparable amplitude in the signal for Cu, attributable to mottled chalcopyrite disease. (c) Sacarimb (Sac 77.4). Note irregular signals for Pb, Sb, Bi and Tl, all chiefly present in sulfosalt inclusions. (d) Magura (Mag-8). Note correlation between high Au and Te.

our knowledge, the highest reported for sphalerite. Proximity to the inferred fluid source and temporal formation of early Fe and late Zn zones (as interpreted from other characteristics of the orefield; Ciobanu and Cook, 2004) correlates with variation in the In content of sphalerite. This is highest in the Fe zone (mean 86 ppm) and lowest in the Zn zone from the distal Paulus orebody (mean 0.1 ppm); with intermediate concentrations in the Zn zone from proximal orebodies (mean 17 ppm).

The four samples studied from *Baita Bihor* reveal both common trends and pronounced differences. Sample BB 16C contains a very low-Fe-sphalerite. Most elements display flat profiles – Mn, Co, Cd, In and Se are anomalous. Low-Fe-sphalerite from bornite–sphalerite symplectites from the inner part of the same pipe (BB19CB) displays similar element trends and narrow variances. Concentrations of Co are comparable with those of Fe and Mn (mean 1183 ppm), whereas In concentrations are among the highest reported in this paper (mean 812 ppm). The very high In concentrations in sample BB19CB correlate with the previous identification of roquesite in samples from the same location (Cook and Ciobanu, 2003a), and the high Co contents with the presence of discrete Co-bearing sulfides. Anomalous Se and Ag are noted, but other elements, including Bi and Pb, are very low. A third sample (BB6), from deeper in the northern branch of the same pipe has values of most elements similar to BB6C but distinctly higher In values (mean 223 ppm; Fig. 4d). Sphalerite in a fourth sample, from distal Pb–Zn skarn (Marta ore pipe) shows a very different geochemistry, with In and Co contents only in the low tens of ppm, but >100 ppm Se. A feature of the Baita Bihor sphalerite is the very constant concentrations of Co, In, etc. within a single sample, in contrast to the marked variation between samples, which would appear to reflect position within the deposit, and possibly also the speciation and abundance of coexisting phases. Sphalerite in *Valea Seaca* (VS 1b) has comparable concentrations.

The two samples from *Baisoara* (Bs7a and Bs7g) are from the same carbonate-hosted Zn–Pb ore (Cacova Ierii orebody). The high Cd concentrations, and oscillatory zoning in sample Bs7a are not mirrored by high concentrations of any other elements – or a clear correlation with any of them. Both Baisoara samples are, however, one of the few cases where Tl concentrations (13 and 39 ppm) exceed mdl. Furthermore, unlike most of other skarn samples, where Ag, Pb, Sb and Bi concentrations vary across profiles, reflecting abundant inclusions, the contents of Ag in Bs7a

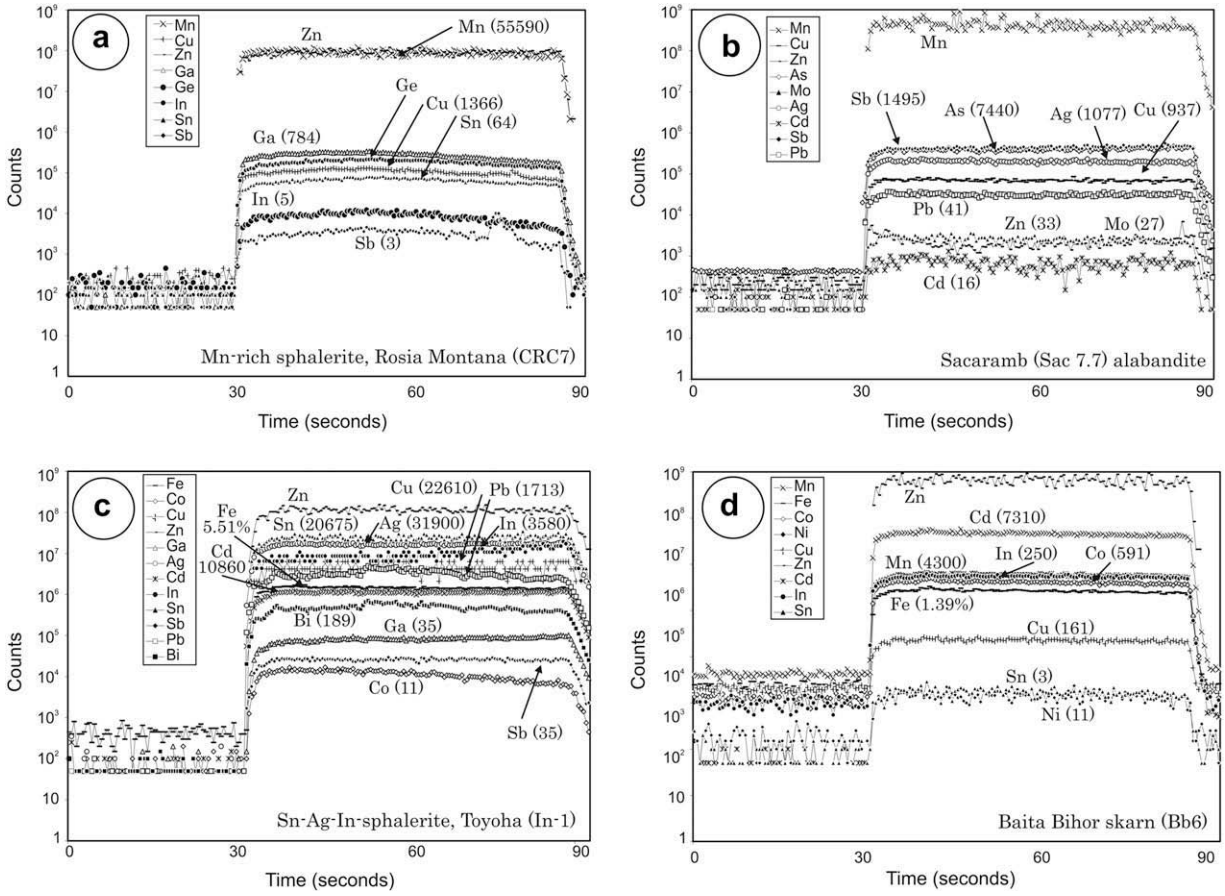

Fig. 4. Representative single-spot LA-ICPMS spectra for selected elements in sphalerite (a, c and d) and alabandite (b). Numbers in brackets are concentrations (in ppm). (a) Rosia Montana (CRC-7). Note high concentrations of Mn, Ga, Ge, Sn and smooth signals for all elements. (b) Sacarimb (Sac 7.7). Note smooth spectra for As, Mo, Sb, Ag, Cu and Pb. (c) Toyoha (In-1, from high Sn–Ag-band within In-sphalerite). Note smooth profiles for all elements, including In, Cu, Pb, Bi and Ga, despite the typical presence of cassiterite inclusions in such zones. (d) Baita Bihor (BB6). Note smooth spectra for all elements.

(mean 46 ppm), Pb (mean 436 ppm), Sb (mean 25 ppm) and Bi (mean 25 ppm) are also more homogeneous in this sample, suggesting that they are in solid solution (Fig. 5a).

Sphalerite from the Late Cretaceous skarns in BMMB shows some common characteristics (e.g., high Mn contents; relatively high In for higher-temperature and/or source-proximal associations), even if there are differences between samples from the same deposit and across the belt. Some of the samples are enriched in both In (e.g., Majdanpek, Baita Bihor) or Co (e.g., Baita Bihor, Ocna de Fier 3375). Notably, however, Ge, Ga and Sn are not enriched in any sample, contrasting markedly with the epithermal ores. The variability within the four samples from the Baita Bihor deposit, five from Ocna de Fier and two from Baisoara suggests caution should be exercised in extrapolating the data from a limited number of samples to a whole deposit. As seen from these skarn examples, concentrations of some trace elements in sphalerite, e.g., In, have potential as markers of orefield zonation in magmatically-driven hydrothermal systems.

The specimen from *Kamioka* shows rather flat profiles for most elements, without noticeable inter-element correlations. Like most other skarns, there is some Mn present, moderately high Co (222–245 ppm) and Cd and variable Ag (1.7–94 ppm). The ragged LA-ICPMS profiles for Ag, as well as the rather irregular spectra for Pb and Bi, with standard deviation exceeding the mean concentration value, suggest the presence of submicro-scale inclusions, not visible in the back-scattered electron images.

The small *Lefevre* skarn features elevated Fe- (10.4 wt.%) and Mn-rich sphalerite, with significant In contents (mean 180 ppm) that correlate with Cu, as well as skarn-characteristic enrichment in Co and deficiency in Ga and Ge.

The main feature of the *Konnerudkollen* Zn skarn (sample Ko99-2) is the erratic values of Ag, Pb and Bi, consistent with the abundant sulfosalt inclusions in the common sulfides. Fluid inclusion data (Segalstad and Telstø, 2002) indicate this is a relatively low-temperature skarn deposit.

5.3. Stratabound deposit types

The two samples from low-temperature carbonate-replacement deposits on Svalbard give values that differ from one another. Elevated As and Ga are noted in *Sinkholmen* sphalerite. Sphalerite from *Kapp Mineral* has

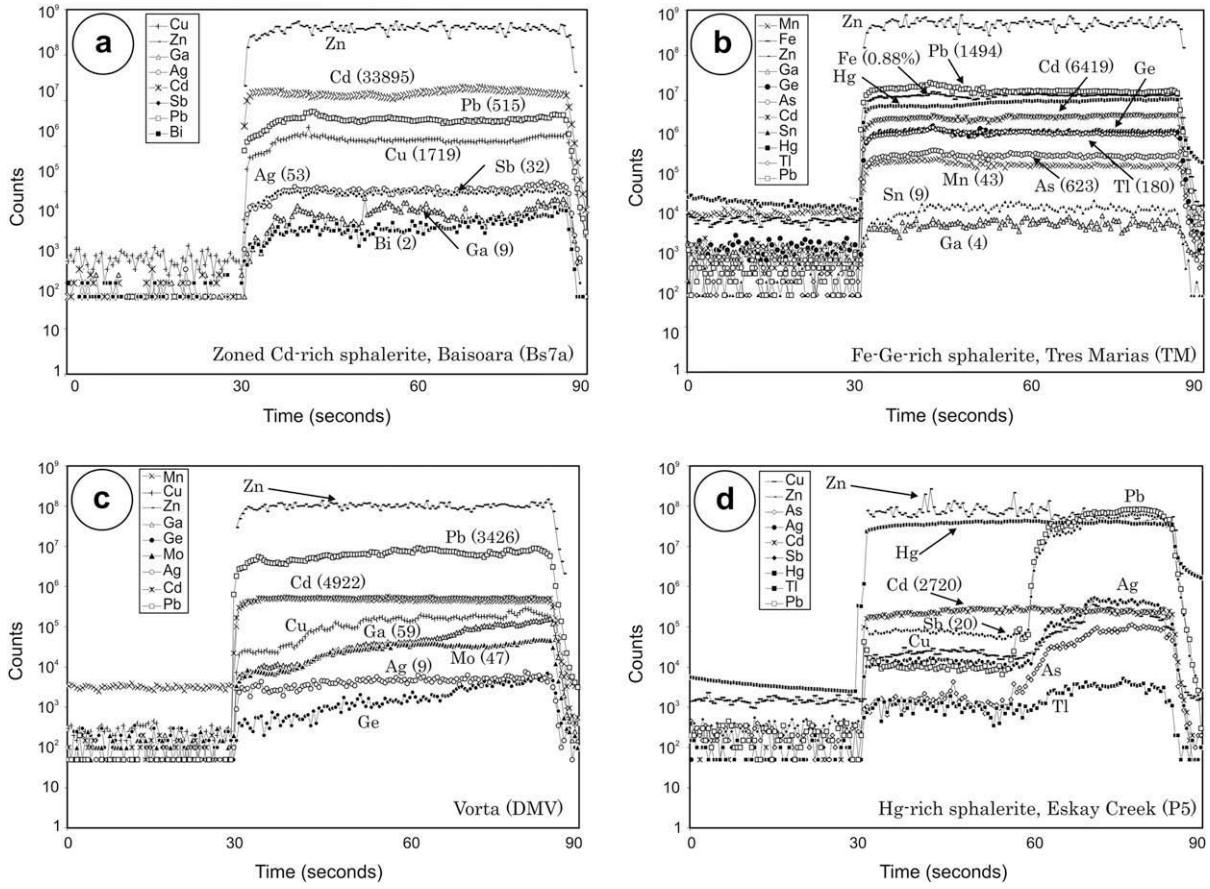

Fig. 5. Representative single-spot LA-ICPMS spectra for selected elements in sphalerite. Numbers in brackets are concentrations (in ppm). (a) Baisoara (Bs7a, Cd-rich sphalerite). Note smooth signals for Pb, Ag and Sb, elements that otherwise show irregularities. (b) Tres Marias (TM). Note smooth profiles for all elements and enrichment in Ge, As, Tl, Hg and Sn. (c) Vorta (DMV). Note relatively high levels of Mo, Ga and Ge, and gradual increase in these elements with crater depth, as well as steady Pb and Ag signals. (d) Eskay Creek (P5, Hg-rich sphalerite). Note smooth signals in first portion of the spectra and then increases in Pb, Sb, Ag, As, Cu and Tl as the crater intercepts a sulfosalt inclusion.

higher Ge content. Enhanced Pb and Ag values, and small peaks on the LA-ICPMS profiles are readily correlated with micro-inclusions of galena within sphalerite.

Analytical data for sphalerite from *Tres Marias* is listed for both the of Ge–Fe-rich and Ge–Fe-poor varieties in Table 3. The Ge-rich variety also contains appreciable quantities of As (520 ppm), Tl (150–160 ppm) and Hg (Fig. 5b). The Ge-poor part of the sample contains lower concentrations of As and Tl, but higher Sb values.

The sample from *Vorta* (DMV) has low concentrations of most elements. This stands out, however, with the highest Mo concentrations in the dataset (mean 58 ppm; Fig. 5c), considerable enrichment in Ga (mean 96 ppm), and also smooth signals for Pb and Ag.

The sample containing Hg-bearing sphalerite from the *Eskay Creek* VMS deposit (P5) had been studied by Grammatikopoulos et al. (2006). Sphalerite contains 0.08–16.35 wt.% Hg, displaying a perfect inverse correlation with Zn, and a diffuse correlation with Fe. Sphalerite within the sample features high, but varied concentrations of Pb, Sb, Ag, Cu, As and Tl, with ragged profiles for all these elements, coincident with inclusions of tetrahedrite–tennantite, Cu–Pb sulfosalts and galena (Fig. 5d). Other elements (Ga, In) also display high variance and ragged profiles suggesting they may not only be hosted within sphalerite, but also in the included minerals.

Samples from *Zinkgruvan*, *Kaveltorp* and *Marketorp* show significant variation. Indium and Se are both higher in the Marketorp sample. Cobalt concentrations are more than an order of magnitude higher in Zinkgruvan and Marketorp than in Kaveltorp.

The relatively high (for a massive sulfide deposit) In concentration in sphalerite from the *Sauda* sample (29 ppm) correlates with the identification of In-bearing sphalerite in another sample from the deposit. The sample also stands out by a mean content of 119 ppm Se in sphalerite.

The sample from a small showing in the Melandsgruve orefield, Hitra, Norway, shows few distinguishing characteristics. Enrichment in As, Sb and Cu is coincident with the abundance of small inclusions of tetrahedrite–tennantite.

5.4. Distributions of individual elements

Indium concentrations are summarized as histograms in Fig. 6a. Seven samples have mean concentrations that

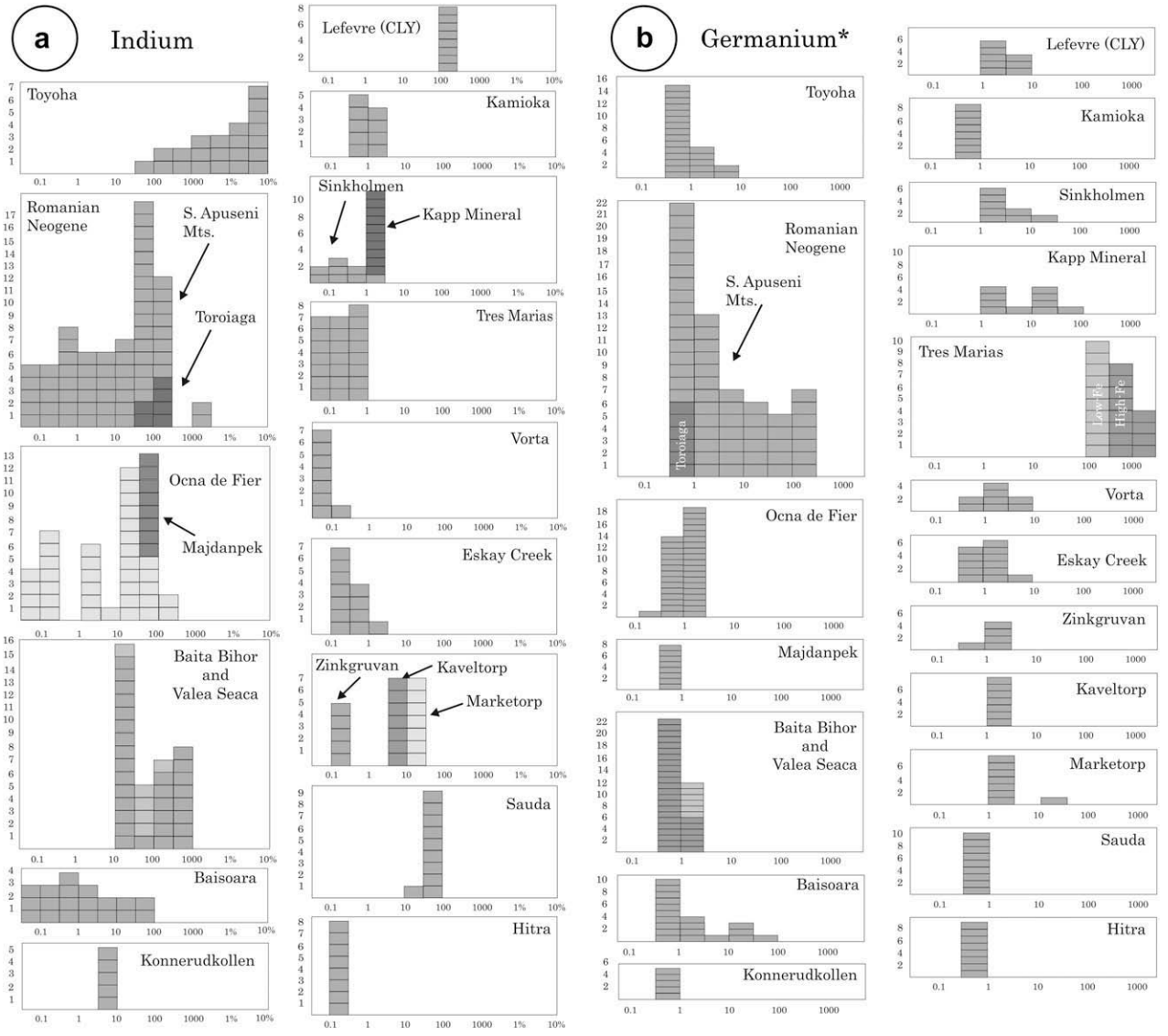

Fig. 6. Histograms showing the distribution of (a) In and (b) Ge* in sphalerite as determined by LA-ICPMS. **Note:* Ge concentrations (in ppm terms) must be considered approximate (see Section 4).

exceed 100 ppm (In-1, In-2, BdA, L-82, BB6, BB19CB, Lefevre L-12). These samples have in common proximity to a presumed magmatic source. In general, skarns and epithermal deposits formed towards the upper end of the temperature range have higher concentrations of indium. In all cases, LA-ICPMS profiles for indium are flat, indicating homogeneity on the scale of the ablation crater, and implicitly, occurrence of the element in solid solution. With few exceptions, standard deviations within each sample are <10% relative to the mean for that sample, indicating homogeneity within the sample. Indium concentrations show a positive correlation with Cu (see Section 6).

Germanium concentrations are generally lower than those of In and, on the scale of the whole dataset, typically enriched in those samples which are poor in In. Concentrations summarized in Fig. 6b show that alongside sample TM, only some of the samples from the GQ are anomalous for the element. LA-ICPMS signals for Ge are smooth throughout the dataset.

In Section 4, we noted that ppm concentrations could not be given with confidence for Ge. Study of the Tres Marias sphalerite presents an opportunity to compare LA-ICPMS data with the electron probe data presented by Saini-Eidukat et al. (2009). Our approximate Ge concentrations in the Ge–Fe-rich sphalerite are somewhat higher, but similar order of magnitude, as the means of 797 ppm (S.D. 318 ppm) and 468 ppm (S.D. 286 ppm) given by Saini-Eidukat et al. (2009) for high- and low-Fe varieties of Type I sphalerite.

Cadmium is a ubiquitous component of all analyzed sphalerite, and unlike other elements – and with exception of oscillatory-zoned Cd-sphalerite in sample Bs7a (up to 12.6 wt.%), Cd concentrations are at the same order of magnitude (1000–10,000 ppm) across the dataset (Fig. 7a);

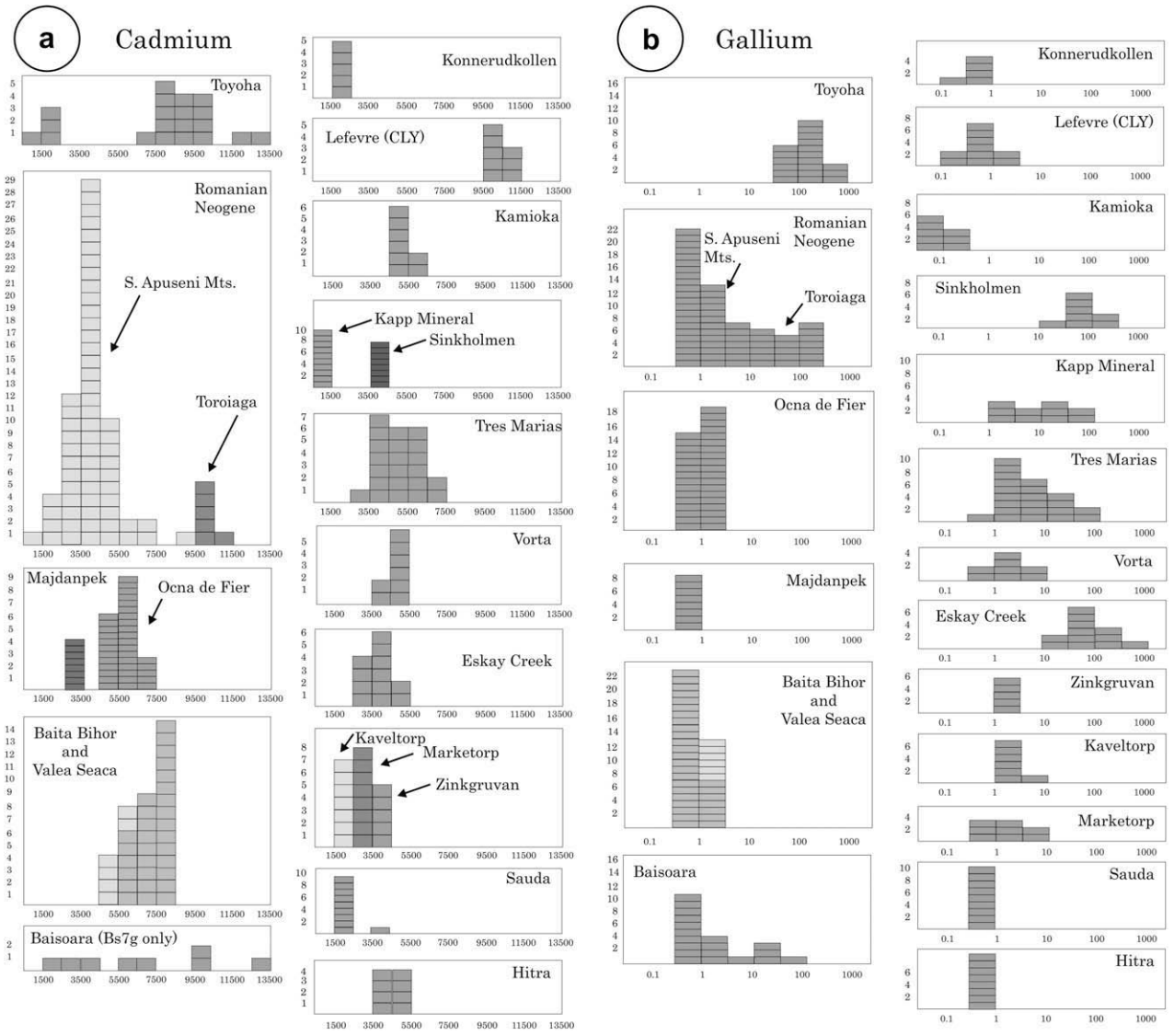

Fig. 7. Histograms showing the distribution of (a) Cd and (b) Ga in sphalerite as determined by LA-ICPMS.

LA-ICPMS profiles are always smooth, implying homogeneous distribution within solid solution.

Gallium concentrations rarely exceed 100 ppm (Fig. 7b). Samples In-1 and In-2 (Toyoha) are anomalous for the element, as are some samples from the GQ, in this case, partly overlapping those enriched in Ge. Several of the carbonate-replacement and VMS deposits are also enriched; skarns are universally low in Ga.

Cobalt appears to be systematically enriched in skarn sphalerite relative to other deposit types, especially epithermal ores (Fig. 8a). Our study has generated some of the highest reported concentrations, notably from Baita Bihor and Ocna de Fier, but also in other skarns (e.g., Konnerudkollen). Moderate concentrations may be anticipated in some stratabound deposits.

Mean concentrations of *selenium* vary across three orders of magnitude, with the dataset offering few clear distribution patterns (Fig. 8b). Samples with higher Se include Sauda (VMS), Kamioka and Majdanpek (skarns) and Larga (epithermal). In these cases, the smooth profiles suggest that Se is lattice-bound (solid–solution). In a few cases, e.g., some spots on samples from Ocna de Fier, elevated Se, appears related to inclusions of discrete Se-bearing minerals.

Mean concentrations of *copper* range from several tens to tens of thousands of ppm. In the majority of samples, the spectra are ragged, clearly showing the presence of Cu-bearing inclusions. This is particularly evident in those samples where sphalerite contains abundant chalcopyrite disease (e.g., Hanes, Baia de Aries). In samples with appreciable In content, the Cu signal is steady.

Several samples are characterized by enrichment in *manganese*, with mean concentrations ranging over three orders of magnitude (hundreds of ppm to several wt.%). Smooth profiles and generally low variability within datasets for individual samples point to incorporation in solid solution within the limits set by experimental work (see above).

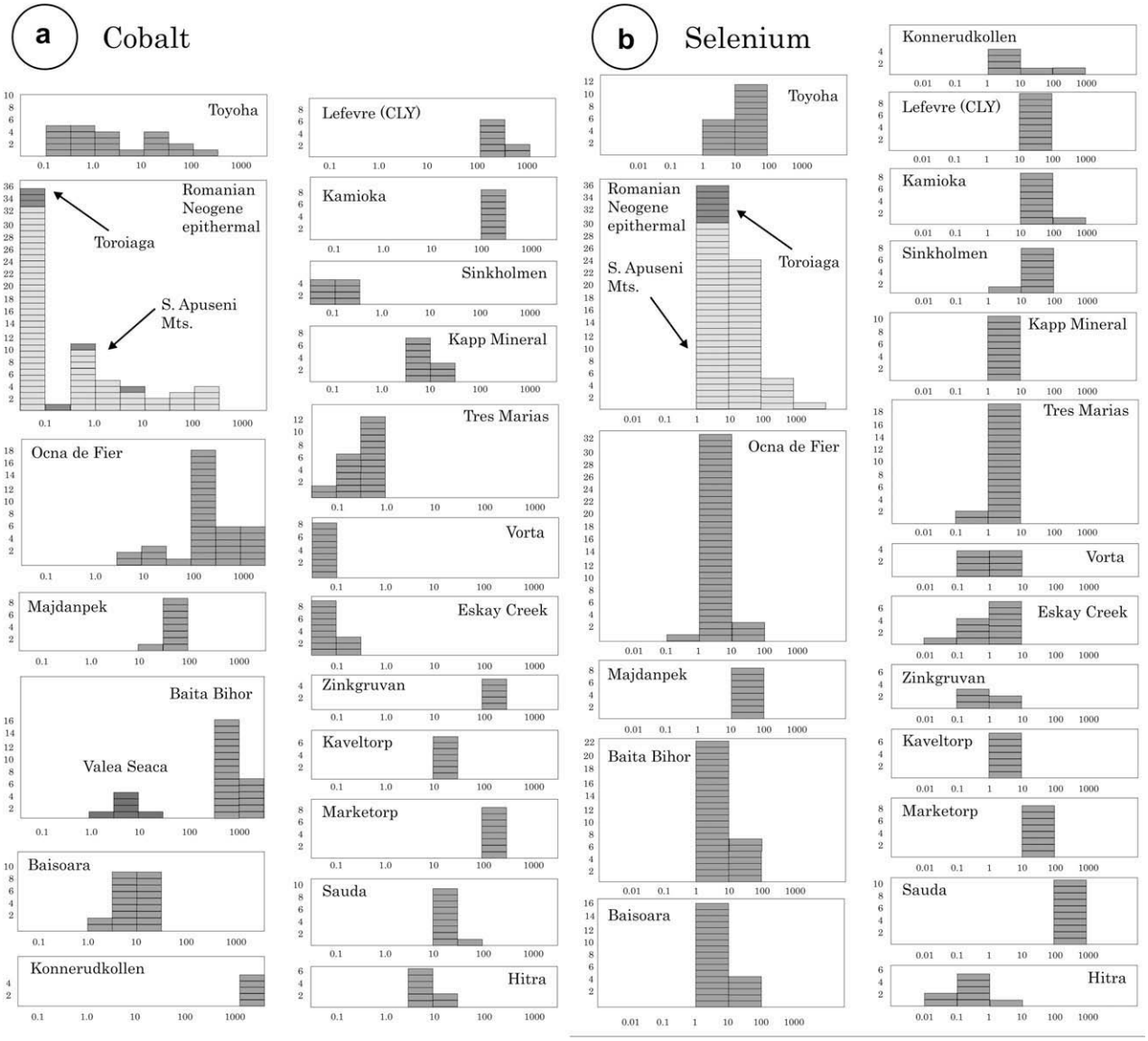

Fig. 8. Histograms showing the distribution of (a) Co and (b) Se in sphalerite as determined by LA-ICPMS.

Patterns of *silver* distribution mirror those of Cu. In the majority of samples (all genetic types) – though not all – LA-ICPMS profiles for Ag are ragged and, in many cases, clearly linked to the presence of Ag-bearing mineral inclusions (galena, tetrahedrite–tennantite, other sulfosalts) rather than solid solution silver. Although several other samples are also suggestive of solid solution silver, the best example is the Indium- and Sn-rich sphalerite (Toyoha), showing solid solution Ag at concentrations of thousands or tens of thousands ppm.

Concentrations of *tin* are low in most samples, notably skarns and stratabound deposits. Concentrations of tens or low hundreds of ppm are, however, not uncommon in the epithermal deposits and the LA-ICPMS profiles suggest incorporation in solid solution. The In-rich specimen from Toyoha is a marked exception to the generally low concentrations, with concentrations of thousands of ppm in In-rich areas, and >1 wt.% in the Sn-rich bands. Smooth profiles and low variability within these data subsets point to incorporation via solid solution (see Section 6).

Like silver, *lead*, and commonly also *bismuth* and *antimony* show considerable enrichment across the dataset. High variability between individual ablation spots and ragged profiles, however, imply that these elements are not generally present in solid solution, but rather as submicro- to nano-scale inclusions of other sulfides or sulfosalts, corroborated by good correlations between the elements in question, and also Cu where tetrahedrite–tennantite or Pb–Cu sulfosalts are present. Steadier profiles in a number of samples (e.g., Bs7a, TM) do, however, suggest that low levels of these elements could enter solid solution in isolated cases.

We were only able to obtain *arsenic* concentrations on part of the sample suite. Tres Marias stands out as the only

sample incorporating hundreds of ppm As within solid solution in sphalerite. We would anticipate that As is also higher in comparable, low-temperature replacement-style deposits. The element appears low in most epithermal and skarn deposits where we were able to obtain data. *Molybdenum* concentrations are <mdl in most sphalerites, and no more than a few ppm in others; sample DMV (Vorta) alone shows concentrations in the tens of ppm range. *Thallium* concentrations are at or close to mdl in most samples. Exceptions include specimens from Baisoara and Tres Marias, where the element is apparently in solid solution. Ragged profiles for Tl (e.g., in Sacarimb or Eskay Creek) are best attributable to sulfosalt inclusions. Concentrations of *nickel* are low across the dataset, rarely exceeding a few ppm; concentrations are higher in samples also enriched in Co (e.g., BB6, Fig. 4c). Concentrations of *tellurium* and *gold* (not included in Table 3) lie at, or below mdl (~0.05 ppm) in all specimens, except in Magura and Sacarimb (see Section 5.1).

6. DISCUSSION

6.1. Element distribution and correlation trends

The dataset shows a marked correlation trend between Cu and In, with a slope of ~1, as would be expected from the coupled substitution mechanism $2Zn^{2+} \leftrightarrow Cu^{+} + In^{3+}$ (Fig. 9a). This is particularly valid for the samples with the highest In contents. The presence of In^{3+} is generally assumed, even if mixed-valence In-chalcogenides are known (Epple et al., 2000). The In charge still has to be proven using appropriate methods (EXAFS, XPS). The trend on Fig. 9a is, however, partially obscured by the volume of data that plot above the correlation line, i.e., with elevated Cu, but lower In. Such data (e.g., from the stratabound or Romanian epithermal deposits) are characterized by abundant excretions of chalcopyrite, which can be presumed to extend from the micro-scale to the nano-scale; these sphalerites are also enriched in Fe. It is notable, however, that sphalerite from several skarn samples plot very close to the correlation line.

A second strong positive correlation is observed between Ag and Sn, especially for the In-rich sphalerite from Toyoha, where the two elements are present in solid solution and in approximately equal proportions (Fig. 9b). This implies that these two elements are also involved in a coupled substitution. Such an interpretation also implied by the distribution of Ag and Sn in sample In-1, in which bands rich in these elements are clearly distinct from the Cu–In-rich bands. Coupled substitution of the type $2Zn^{2+} \leftrightarrow Ag^{+} + Sn^{3+}$ is difficult to validate without evidence for a reduced state of Sn in sphalerite (normally as Sn^{4+}), but this might be inferred from the data. Such an interpretation, or indeed the presence of Sn^{2+}, needs to be verified by, for example, XPS analysis. Alternatively, if Sn is present as Sn^{4+}, substitution mechanisms may involve vacancies, for example, $2Zn^{2+} \leftrightarrow \square + Sn^{4+}$. A further alternative substitution mechanism would be $3Zn^{2+} \leftrightarrow 2(Ag,Cu)^{+} + Sn^{4+}$. The gross distributions of Cu, In, Ag and Sn in sample In-1 suggests that the two coupled substitutions act, at least partly, independent of one another, and relate to the two distinct zoning patterns within the specimen.

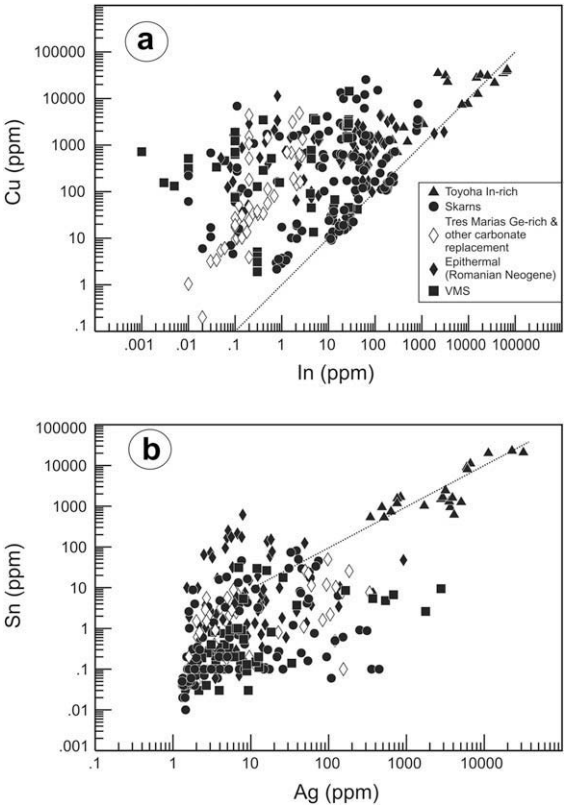

Fig. 9. Correlation plots of (a) Cu *vs.* In, and (b) Sn *vs.* Ag in sphalerite from the total dataset. Dashed lines represent 1:1 correlations between concentrations (ppm). On (a), the positive correlation trend between Cu and In is partially obscured by those data that plot above the 1:1 correlation line. These are from samples characterized by abundant excretions of chalcopyrite. See text for additional explanation.

The dataset reveals a number of positive or negative inter-element correlations, though these are often diffuse due to the heterogeneous character of our sample suite. For example, Fig. 10a shows a possible weak inverse correlation between concentrations of In and Ge in sphalerite, with those specimens or ore types enriched in In being deficient in Ge, and vice versa; any sense of negative correlation disappears however, if the Tres Marias data are excluded. This is also true for Ga, which is generally lower in In-rich specimens, even if the high-In sample from Toyoha is moderately enriched in Ga. Hence there is a weak positive correlation between Ga and Ge (Fig. 10b) for most of the dataset. This may rather indicate that sources enriched in one element are generally also enriched in the other, even if the dataset is somewhat biased, and the correlation accordingly amplified, by the Ga- and Ge-rich sphalerites from Romania. Fig. 10b shows, however, a marked negative correlation between the two elements in the data for Tres Marias and other carbonate-replacement deposits (Fig. 10b), with the high-Fe–Ge parts of the sample having Ga concentrations an order of magnitude lower than the low-Fe–Ge parts. We are unable to explain this, but suggest

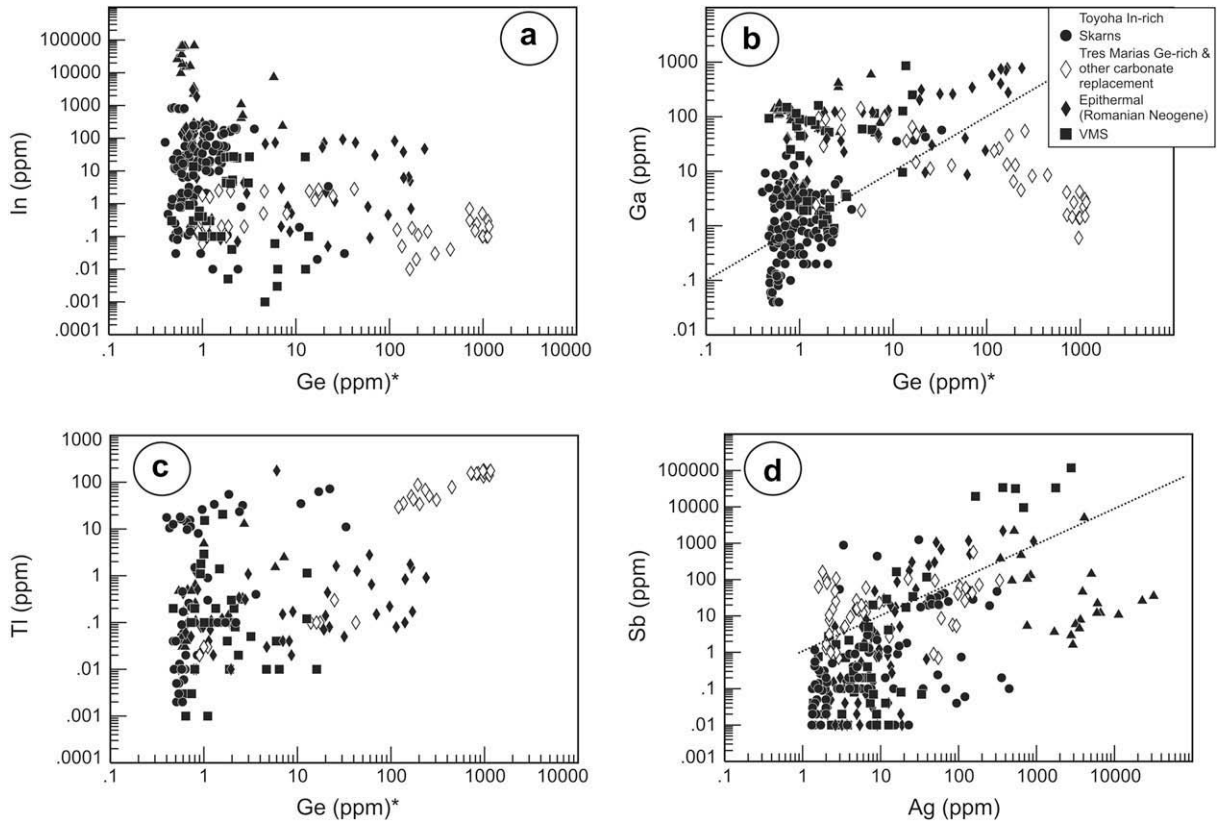

Fig. 10. Correlation plots of (a) In *vs.* Ge*, (b) Ga *vs.* Ge*, (c) Tl *vs.* Ge*, and (d) Sb *vs.* Ag in sphalerite from the total dataset. See text for explanation. Dashed lines on (b) and (d) represent theoretical 1:1 correlations. **Note:* Ge concentrations (in ppm terms) must be considered approximate (see Section 4).

it may be a statistical artifact generated by our disparate sample suite. Thallium is also generally enriched in the Ge-richer deposits, giving the weak positive correlation between the two elements seen in Fig. 10c.

The weak correlation between Ag and Sb in the total dataset (Fig. 10d) suggests a possible role for a limited degree of $2Zn^{2+} \leftrightarrow Ag^{+} + Sb^{3+}$ substitution, alongside solid solution silver in the In- and Sn-rich specimens and the nano-scale inclusions of Ag–Sb-bearing minerals. The weak correlations between Ag and both Pb and Bi can best be interpreted in terms of nano-scale inclusions of galena or sulfosalts rather than any coupled substitution at the atomic level, especially given the erratic, inhomogeneous character of the profiles for these elements.

Cobalt and Ni show a positive correlation (Fig. 11a), with a reasonably constant slope of Co/Ni = 10. This correlation appears independent of any potential Co–Fe or Ni–Fe relationships. Iron is the most ubiquitous minor element in sphalerite. Plotting individual elements against Fe should, therefore, indicate if the presence of Fe assists incorporation of other components. Relationships between Fe and Mn (Fig. 11b) show little general trends, but weak positive correlation between the two elements in individual deposit- or sample-subsets, is at odds with suggestions of an inverse correlation between the two (Di Benedetto et al., 2005). The good correlation between Fe and Ge seen in the Tres Marias sphalerite (Fig. 11c) is not borne out across the full dataset, with even a suggestion of a negative correlation between the two elements among the Romanian Neogene epithermal deposits. Except some of the skarn deposits, which cluster astray from the bulk of the data points, there is a broad correlation between Co and Fe (Co/Fe ~ 1000; Fig. 11d).

It is clear from the high degree of variance within the dataset that rather than elements showing universal strong positive or negative correlations with one another, each sample or group of samples with comparable characteristics in terms of source and genetic type, has a distinct geochemical signature expressed in elevated concentrations of one or more elements. This is evident, for example, within the Romanian Neogene epithermal deposits, where some samples show enrichment in Ga and Ge, others in Ge and In and others in only one of the three elements.

6.2. Substitution mechanisms

The data obtained do not contradict established substitution mechanisms for minor elements in sphalerite, especially for Mn, Cd, Co, Ni, where simple substitution of the bivalent cation can be assumed. The dataset also fully supports incorporation of Cu and Ag as monovalent cations, via coupled substitutions, e.g., with In^{3+}, Sb^{3+} and probably also Sn^{3+} or Sn^{4+} as outlined above. More problematic are the substitutions involved for Ga and Ge. One

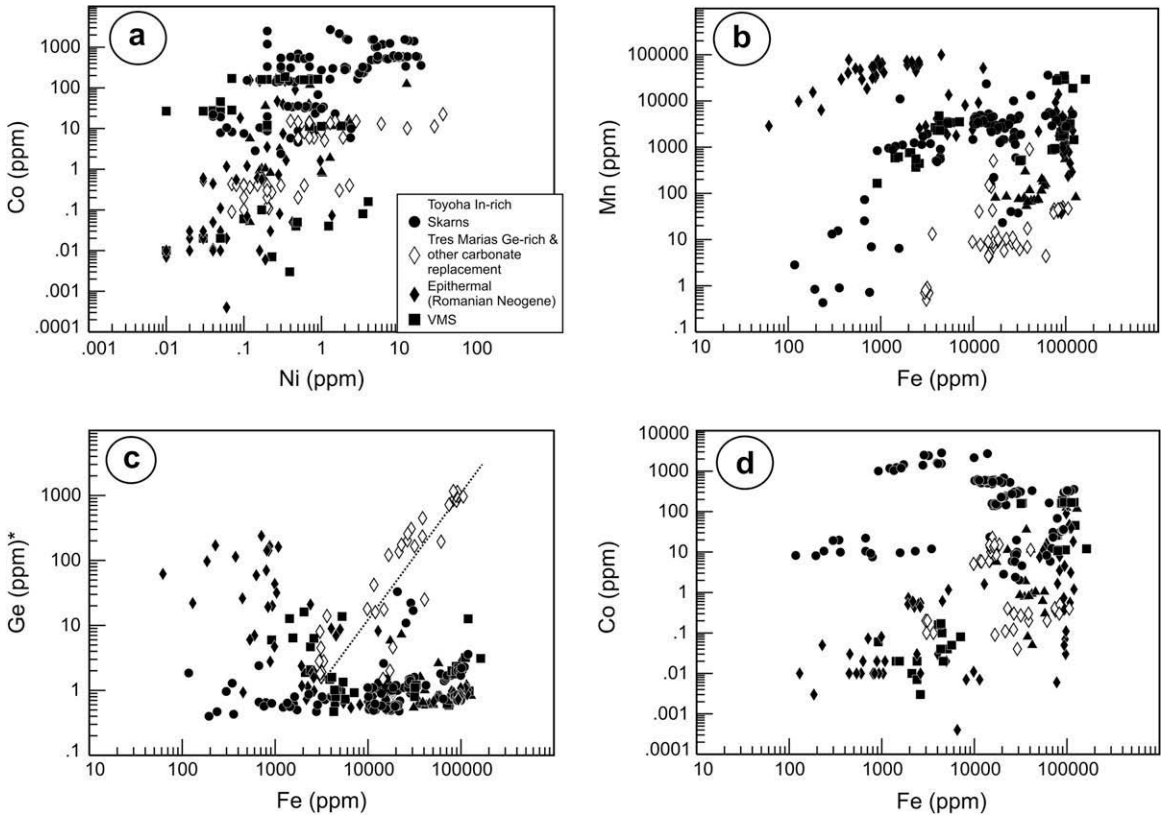

Fig. 11. Correlation plots of (a) Co *vs.* Ni, (b) Mn *vs.* Fe, (c) Ge* *vs.* Fe, (c) Co *vs.* Fe in sphalerite from the total dataset. See text for explanation. Note on (c) the dashed line showing 1:1 correlation showing excellent correlation between Ge and Fe in the data subset for the Tres Marias sample. **Note:* Ge concentrations (in ppm terms) must be considered approximate (see Section 4).

might reasonably expect Ge to be present in the Ge^{4+} state. Johan (1988) proposed coupled substitution mechanisms for trivalent and tetravalent elements (including Ga^{3+}, Sn^{4+} and Ge^{4+}) in sphalerite, leading us to anticipate that analyses with elevated Ge concentrations would also feature enrichment in a monovalent ion (Ag and/or Cu). This is not observed, and indeed the Tres Marias subset shows no enrichment in monovalent ions, making a coupled substitution mechanism of the type proposed by Johan (1988) difficult to envisage. The Tres Marias subset does, however, show correlation between Fe and Ge, with Ge concentrations highest in Fe-enriched positions of the sample. This raises the possibility of a coupled substitution involving Fe and Ge (e.g., $2Fe^{2+} + Ge^{4+} \leftrightarrow 4Zn^{2+}$). Another, straightforward explanation is a simple substitution of Ge in reduced state (Ge^{2+}), although we have no supporting evidence and would need to corroborate such a speculation by establishing the oxidation state of Ge in natural samples. The lack of evidence for a coupled substitution involving Ge^{4+} and a monovalent cation can be seen from the Cu + Ag *vs.* Sn + Ge + Ga + In plot (Fig. 12a). Analyses with chalcopyrite disease or discrete Ag-mineral inclusions notwithstanding (these plot above the line), there is a reasonable correlation between (Cu + Ag) and (Sn + Ge + Ga + In) for a fair proportion of the dataset, but the high-Ge-sphalerite from Tres Marias falls well below the line.

Gallium may be present in trivalent form in that a plot of Ga *vs.* Ag + Cu (Fig. 12b) broadly supports the coupled substitution $(Ag,Cu)^{+} + Ga^{3+} \leftrightarrow 2Zn^{2+}$, at least for a part of the sphalerite population (including those with highest Ga concentrations) where the approach is less complicated by other, independent coupled substitutions of M^{3+} and M^{4+} cations into sphalerite, or by Cu as chalcopyrite disease.

Ohta (1995) recognized a number of solid solutions in the Zn-(Cu + Ag)–(Sn + In) system from Toyoha, principally between sphalerite and $CuZn_2InS_4$, between roquesite and $CuZn_2InS_4$, between chalcopyrite and stannnite, probable kesterite–roquesite and kesterite–sakuraiite solid solutions, as well as evidence for sphalerite–stannite solid solution. The distinct zonation patterns expressed by In(Cu) and Sn(Ag), an earlier (?) Fe-zonation in the sphalerite, and evidence of coupled (Ag–Sn) ↔ Zn substitution in addition to (Cu–In) ↔ Zn coupled substitution, suggest complex phase relationships in the system Ag–Cu–(Fe)–Zn–In–Sn–S. These (e.g., possible partial solid solution between sphalerite and pirquitasite, Ag_2ZnSnS_4, as well as stannite) remain poorly constrained and are beyond the scope of the present contribution.

6.3. Patterning and textures in sphalerite

Oscillatory zonation and rhythmic banding due to incorporation of minor components in sphalerite has been widely

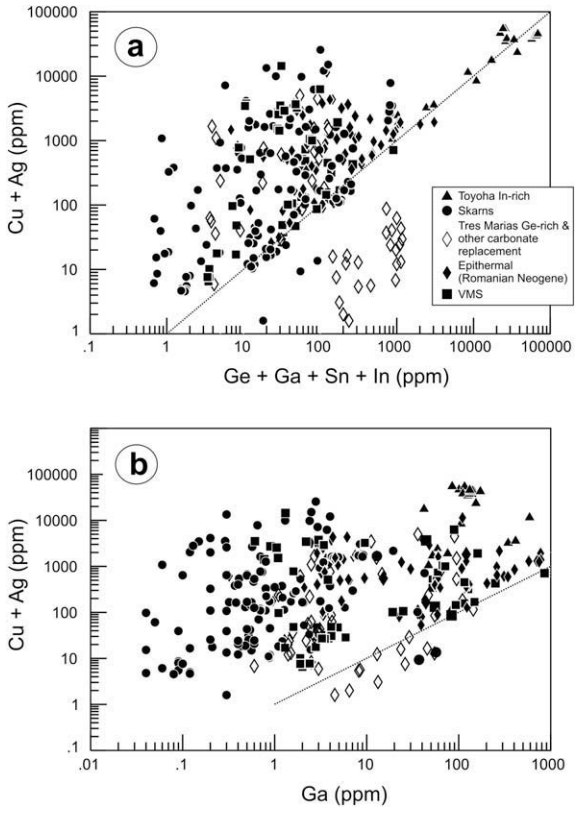

Fig. 12. Correlation plots of (a) Cu + Ag *vs.* Sn + Ge + Ga + In and (b) Cu + Ag *vs.* Ga in sphalerite from the total dataset. Dotted lines show theoretical 1:1 correlation. Note in (a) that although some analyses plot close to the line, many also plot to the left of the line; these feature abundant chalcopyrite disease. The data subset for the Tres Marias sample plots to the right of the line. Note (in b) the good correlation between Ga and Ag + Cu in those analyses without chalcopyrite disease.

reported and interpreted in the literature (e.g., Oen et al., 1980; Pattrick et al., 1993; Fowler and L'Heureux, 1996; Beaudoin, 2000; Di Benedetto et al., 2005). Contradictory interpretations stem from the variety of different compositional patterns observed in natural samples. In the present study, microscopic-scale patterns for minor components such as Fe, Mn, Cd, In and Sn were also found in sphalerite, although not in all cases; intriguing exceptions include Fe-rich sphalerite from skarns, e.g., Paulus/Ocna de Fier, deposits that are typified by such mineral patterns (e.g., Ciobanu and Cook, 2004; Ciobanu et al., 2004c). Involvement of trace elements (<1 wt.%) in the patterning can be suggested in some of the examples, e.g., Ge in Tres Marias, or In, Ag, Sn in distinct zones of the patterns described from Toyoha.

Crystal-structural control on minor/trace element incorporation (e.g., Fe), in particular a series of rotational/inversional twinning and faults characteristic for the cubic, diamond-type structure of sphalerite, was pointed at by HR-TEM studies showing nano-scale oscillatory zonation in Fe-rich sphalerite (Pósfai and Buseck, 1997 and references therein). Similarly, rotational twinning driving nano-scale oscillatory zonation has been identified in low-In-sphalerite (In-1). In subsequent work the present authors will extend such studies, also using focused ion beam method (allowing cutting at specific locations across a given pattern) for HR-TEM sample preparation. This will permit a correlation between trace/minor elements and crystal-structural control of patterning.

Pattern analysis using one of the genetic models involving the 'coarsening wave', applied for example to Fe–Zn banding in sphalerite from MVT deposits (Katsev et al., 2001), is necessary to assess whether the patterning is triggered by intrinsic (self-organization) or external factors. Sphalerite patterns discussed here (i.e., Cd- and In–Sn zonation patterns (Baisoara, Toyoha), mottled 'chalcopyrite disease' (Baia de Aries, Hanes), Fe–Ge patterns (Tres Marias) could be treated using the same models and are considered by the authors in their future work.

6.4. Petrogenetic considerations

The distributions observed across the dataset, and the characteristic element signatures of specific ore provinces (e.g., GQ or BMMB) or individual deposits (e.g., Ocna de Fier), suggest that patterns of minor/trace elements in sphalerite such as In or Ge can be used for petrogenetic interpretation, e.g., orebody/field zonation relative to fluid sources, formation temperature.

Concentrations and fractionation of a given element into sphalerite are influenced by type of deposit (factors such as crystallization temperature, metal source, cooling history, etc.) and, not least, the proportion of sphalerite in the ore and coexistence/absence of discrete minerals containing Mn, Co, In, Ga, Ge, etc. As outlined in Section 5, skarn and some epithermal deposits appear to have higher concentrations of several elements in solid solution, notably In, in cases where the ore is proximally positioned relative to the causative intrusive body, but also Co (especially in the skarns), Sn and Mn and, in some cases, also Ag (e.g., Toyoha). Likewise, Ge, As, Tl, Ga and Se appear enriched in lower-temperature deposits without a magmatic source (e.g., Tres Marias). More unusual signatures of some deposits (e.g., Mo in Vorta) could be interpreted in terms of the local geological setting. Molybdenum might typify ophiolite-hosted mineralization in SAM (presence of Mo-deposits). Alternatively, Mo may result from a Late Cretaceous overprint if this assumed age can be confirmed by dating subvolcanic bodies at Vorta. We note that sphalerite from neither Late Cretaceous skarns (BMMB) nor Neogene deposits (GQ) displays Mo signatures. The Bi-mineral signature in the BMMB is also reflected in the higher Bi concentrations in sphalerite. The Te signature of the Au deposits in the GQ is not reflected in sphalerite, but the exceptional Au content in Magura also correlates with Te.

The minor/trace element variations that correlate so well with the patterns and textures from Toyoha back up the interpretation of In deposition during a high-temperature fluid pulse, i.e., 50–100 °C higher than the ca. 300 °C of the main veins (sub-stage B of the later-stage mineralization, with reworking during the "silver-sulfosalt" sub-stage C; Ohta, 1991). Textures in sample In-1 clearly show that a pre-existing sphalerite ore was affected by replacement due

to percolation of fluids enriched in In, Sn, Ag and As. Features such as oscillatory zoning and symplectites, developed during and after arsenopyrite growth, indicate that this process may have involved coupling between dissolution and reprecipitation (e.g., Putnis, 2002; Ciobanu et al., 2008). The replacement process became erratic in the final stages (patchy porosity, corrosion of arsenopyrite, nucleation of larger Sn, Ag-bearing minerals).

Several authors have identified trace element distributions and suggested that these may be used to discriminate among ore genetic types, or be used as geochemical vectors in exploration. The lack of sufficient comparative data, and until recently, the difficulty of obtaining reliable data has, however, precluded routine application of such methods. Attempts have been made to develop a framework for discrimination of ore genetic types. Trace element data for sphalerite and other sulfides have also been used to identify zonation within an orefield or province (e.g., Monteiro et al., 2006). For some provinces, e.g., Zn–Pb deposits in the Eastern Alps, large volumes of trace element data exist for sphalerite (Viets et al., 1992; Schroll, 1996, 1997; Kuhlemann et al., 2001).

6.5. Ore processing implications

Abraitis et al. (2004) reviewed the chemistry and electrical properties of pyrite and concluded that the highly variable behavior in flotation circuits can be explained by variability in the trace and minor element contents. These authors were unable to establish these links in detail but commented that variable textures and intergrowth characteristics may impact upon electrochemical processes during flotation. There are less comparative data available for sphalerite. Increased Fe content adversely affects sphalerite flotation (Boulton et al., 2005) and it may be expected that Mn, Cd, In, Cu also influence recovery. Even though the form of Au (solid solution or inclusions) in Magura sphalerite needs further investigation, the consistent ppm values emphasize, from a processing point of view, the impact this kind of study has for identifying hitherto ignored Au-carriers.

6.6. Environmental implications

Sphalerite in abandoned ore dumps and mine tailings represents a potential environmental hazard, especially due to the relatively little information on the behavior of toxic trace elements and their dissolution rates relative to bulk reactivity (e.g., Abraitis et al., 2004; Arroyo and Siebe, 2007). Sphalerite is generally considered less reactive than pyrite, but dissolution rates for the two minerals may nevertheless be comparable. Unlike pyrite, sphalerite may even continue dissolving in a non-oxidizing environment (Acero et al., 2007a). During dissolution, a characteristic Zn-deficient layer will be formed at the sphalerite surface (e.g., Buckley et al., 1989; Weisener et al., 2004). The characteristics of the immediate surface layer of sphalerite may differ significantly from the mineral bulk, even in vacuum-cleaved specimens (e.g., Harmer et al., 2007), with implications for both mineral recovery by flotation, and dissolution during oxidative weathering. In mine dumps, mineral surfaces may also represent sites for precipitation of dissolved metals (e.g., Cd dissolved from pyrite on pyrite surfaces; Öhlander et al., 2007). A recent study of Cd and Zn weathering dynamics (Kossoff et al., 2008) has shown dissimilar behavior of the two elements, notably that the Zn/Cd molar ratio in column leachate waters increases fourfold over the first 10 years, before retreating to levels of the unaltered tailings. This type of study (although contrasting with results obtained by other workers, e.g., Acero et al., 2007b), illustrates the necessity and usefulness of benchmark geochemical data on the concentrations of trace elements in the non-weathered minerals.

7. CONCLUSIONS

1. LA-ICPMS methods can accurately characterize trace/minor element contents in sphalerite. The technique allows elements in solid solution to be distinguished from micro-inclusions.
2. Sphalerite from each deposit is characterized by specific ranges (0.2–1.0 wt.%) of Cd concentrations. Higher concentrations are rare; spot analyses in this study showed up to 13.2 wt.% in zones of oscillatory-banded sphalerite. All evidence points to $Cd^{2+} \leftrightarrow Zn^{2+}$ substitution.
3. In-bearing sphalerite (Toyoha, Japan) contains superimposed zoning patterns. In-sphalerite (up to 6.7 wt.% In) coexists with bands of Sn-bearing sphalerite (up to 2.3 wt.%). Indium concentration correlates with Cu, corroborating paired $(Cu^{+}In^{3+}) \leftrightarrow 2Zn^{2+}$ substitution; Sn concentrations correlate best with Ag, suggesting a second $(Ag^{+}Sn^{3+}) \leftrightarrow 2Zn^{2+}$ or $(Ag^{+}Cu^{+}Sn^{4+}) \leftrightarrow 3Zn^{2+}$substitution. Both zonation trends are superimposed onto an earlier (?) Fe-zonation.
4. Ge-bearing sphalerite (Tres Marias, Mexico) displays Ge enrichment that shows a positive correlation with Fe. There is no evidence of coupled substitutions involving monovalent ions, leading to the suggestion that Ge may be present as Ge^{2+} rather than as Ge^{4+}.
5. Samples from different localities show high trace element concentrations, including In, Ge, Ga and Co. Cobalt concentrations approaching 2300 ppm in some specimens are the highest reported.
6. Concentrations of a given element vary significantly between samples and even grains of sphalerite in the same sample. More data are required to support some of the trends identified here and to correlate them with the rules governing sphalerite trace element geochemistry.
7. Fractionation of a given element into sphalerite is influenced by factors such as temperature of crystallization, source of metals and cooling history. Partitioning influenced by the amount of sphalerite and other minerals in the ore (e.g., Bethke and Barton, 1971) may lead to a dilution effect: sphalerite in massive Zn–Pb ores will contain average lower concentrations of, e.g., In, than an ore in which sphalerite is only a minor component.
8. Trace elements concentrations in sphalerite have petrogenetic significance, e.g., In from magmatically-driven hydrothermal systems, for interpretation of orefield zonation.

ACKNOWLEDGEMENTS

The senior author acknowledges funding support via a 3-month visiting fellowship at the Ian Wark Research Institute, University of South Australia, and additional support via a Norwegian Research Council grant for bilateral collaboration between Norway and Japan. C.L.C. acknowledges funding through an Australian Research Council 'Discovery' Grant (DP0560001). Sarah Gilbert (CODES) is warmly thanked for all laboratory assistance during the LA-ICPMS runs. Krister Sundblad, Torfinn Kjærnet and William Howard are warmly 1021 thanked for assistance with fieldwork and sampling in Bergslagen Spitsbergen and CLY (B.C., Canada), respectively. Tassos Grammatikopoulos is gratefully acknowledged for providing specimens from Eskay Creek. N.J.C. wishes to thank Yasushi Watanabe for fruitful discussion on the Toyoha deposit and kindly supplying some of the Japanese literature on the deposit. BSE acknowledges the German-American Fulbright Commission and War Eagle Mining. We much appreciate the helpful comments and suggestions of three journal reviewers and Associate Editor David Vaughan.

APPENDIX A. SUPPLEMENTARY DATA

Supplementary data associated with this article can be found, in the online version, at doi:10.1016/j.gca.2009.05.045.

REFERENCES

Abraitis P., Pattrick R., Kelsall G. and Vaughan D. (2004) Acid leaching and dissolution of major sulphide ore minerals: processes and galvanic effects in complex systems. *Miner. Mag.* **68**, 343–351.

Acero P., Cama J. and Ayora C. (2007a) Sphalerite dissolution kinetics in an acidic environment. *Appl. Geochem.* **22**, 1872–1883.

Acero P., Ayora C. and Carrera J. (2007b) Coupled thermal, hydraulic and geochemical evolution of pyritic tailings in unsaturated column experiments. *Geochem. Cosmochim. Acta* **71**, 5325–5338.

Alderton D. H. M., Simon G., Ioan M., Panazan I., Orlandea E. and Csibi I. (1997) Geochemical studies of gold–silver–tellurium mineralization in the vicinity of Sacaramb, Southern Apuseni Mountains, Romania: some preliminary results. *Rom. J. Mineral.* **78**, 31–38.

Alfantazi A. M. and Moskalyk R. R. (2003) Processing of indium: a review. *Miner. Eng.* **16**, 687–694.

Andersson M., Cook N. J., Korneliussen A. and Ottesen R. T. (2004) Saudaprosjektet – Tipp Raundalen. Mulige miljøkonsekvenser ved deponering av sinkholdig malm. Norges geol. Unders. Report 2004.029, 15pp.

Arroyo Y. R. R. and Siebe C. (2007) Weathering of sulphide minerals and trace element speciation in tailings of various ages in the Guanajuato mining district, Mexico. *Catena* **71**, 497–506.

Axelsson M. D. and Rodushkin I. (2001) Determination of major and trace elements in sphalerite using laser ablation double focusing sector field ICP-MS. *J. Geochem. Explor.* **72**, 81–89.

Barreau N. (2008) Indium sulfide and relatives in the world of photovoltaics. *Solar Energy*. doi:10.1016/j.solener.2008.08.008.

Barton, Jr., P. B. and Bethke P. M. (1987) Chalcopyrite disease in sphalerite: pathology and epidemiology. *Am. Mineral.* **72**, 451–467.

Beaudoin G. (2000) Acicular sphalerite enriched in Ag, Sb, and Cu embedded within colour banded sphalerite from the Kokanee Range, BC. *Can. Mineral.* **38**, 1387–1398.

Becker W. and Lutz H. D. (1978) Phase studies in the systems CoS–MnS, CoS–MnS, and CoS–CdS. *Mater. Res. Bull.* **13**, 907–911.

Benzaazoua M., Marion P., Pinto A., Migeon G. and Wagner F. E. (2003) Tin and indium mineralogy within selected samples from the Neves Corvo ore deposit (Portugal): a multidisciplinary study. *Miner. Eng.* **16**, 1291–1302.

Bernardini G. P., Borgheresi M., Cipriani C., Di Benedetto F. and Romanelli M. (2004) Mn distribution in sphalerite: an EPR study. *Phys. Chem. Miner.* **31**, 80–84.

Bernstein L. R. (1985) Germanium geochemistry and mineralogy. *Geochim. Cosmochim. Acta* **49**, 2409–2422.

Bethke P. M. and Borton, Jr., P. B. (1971) Disribution of some minor elements between coexisting sulphide minerals. *Econ. Geol.* **66**, 140–163.

Boulton A., Fornasiero D. and Ralston J. (2005) Effect of iron content in sphalerite on flotation. *Miner. Eng.* **18**, 1120–1122.

Buckley A., Wouterlood H. and Woods R. (1989) The surface composition of natural sphalerites under oxidative leaching conditions. *Hydrometallurgy* **22**, 39–56.

Burke E. A. J. and Kieft C. (1980) Roquesite and Cu–In-bearing sphalerite from Långban, Bergslagen, Sweden. *Can. Mineral.* **18**, 361–363.

Butler I. B. and Nesbitt R. W. (1999) Trace element distributions in the chalcopyrite wall of a black smoker chimney: insights from laser ablation inductively coupled plasma mass spectrometry (LA-ICP-MS). *Earth Planet. Sci. Lett.* **167**, 335–345.

Cabri L. J., Campbell J. L., Laflamme J. H. G., Leigh R. G., Maxwell J. A. and Scott J. D. (1985) Proton-microprobe analysis of trace elements in sulfides from some massive-sulfide deposits. *Can. Mineral.* **23**, 133–148.

Cassard D., Chabod J. C., Marcoux E., Bourgine B., Castaing C., Gros Y., Kosakevich A., Moisy M. and Viallefond L. (1996) Mise en place et origine des minéralisations du gisement à Zn, Ge, Ag, (Pb, Cd) de Noailhac – Saint-Salvy (Tarn, France). *Chron. Recherche Miniére* **514**, 3–37.

Chen W. W., Zhang J. M., Ardell A. J. and Dunn B. (1988) Solid-state phase equilibria in the ZnS–CdS system. Technical Report No. 1, UCLA, Dept. of Materials Sci. Eng.

Chryssoulis S. L. and Surges L. J. (1988) Behaviour of tetrahedrite in mill circuits of Brunswick mining and Smelting Corporation Ltd.. In *Silver Exploration, Mining and Treatment*. Inst. Mining Metall, London, pp. 205–216.

Ciobanu C. L. and Cook N. J. (2000) Intergrowths of bismuth sulphosalts from the Ocna de Fier Fe-skarn deposit, Banat, Southwest Romania. *Eur. J. Mineral.* **12**, 899–917.

Ciobanu C. L. and Cook N. J. (2004) Skarn textures: a case study of the Ocna de Fier-Dognecea orefield, Banat, Romania. *Ore Geol. Rev.* **24**, 315–370.

Ciobanu C. L., Cook N. J. and Ivăşcanu P. M. (2001) Ore deposits of the Vorţa-Dealul Mare area, South Apuseni Mts., Romania: textures and a revised genetic model. *Rom. J. Miner. Dep.* **79**(Suppl. 2), 46–47.

Ciobanu C. L., Cook N. J. and Stein H. (2002) Regional setting and geochronology of the Late Cretaceous Banatitic Magmatic and Metallogenic Belt. *Mineral. Deposita* **37**, 541–567.

Ciobanu C. L., Găbudeanu B. and Cook N. J. (2004a) Neogene ore deposits and metallogeny of the Golden Quadrilateral, South Apuseni Mountains, Romania. In *Gold-Silver-Telluride Deposits of the Golden Quadrilateral, South Apuseni Mts., Romania. IAGOD Guidebook Series*, vol. 12. pp. 23–88.

Ciobanu C. L., Cook N. J., Tamas C., Leary S., Manske S., O'Connor G. and Minut A. (2004b) Tellurides-gold-base metal association at Roşia Montană: the role of hessite as gold

carrier. In *Gold-Silver-Telluride Deposits of the Golden Quadrilateral, South Apuseni Mts., Romania. IAGOD Guidebook Series*, vol. 12. pp. 187–202.

Ciobanu C. L., Pring A. and Cook N. J. (2004c) Micron- to nanoscale intergrowths among members of the cuprobismutite series and padraite: HRTEM and microanalytical evidence. *Mineral. Mag.* **68**, 279–300.

Ciobanu C. L., Cook N. J., Pring A., Damian G. and Capraru N. (2008) Another look at nagyágite from the type locality, Săcărîmb, Romania: replacement, chemical variation and petrogenetic implications. *Mineral. Petrol.* **93**, 273–307.

Ciobanu C. L., Cook N. J., Pring P., Brugger J., Danyushevsky L. and Shimizu M. (2009) 'Invisible gold' in bismuth chalcogenides. *Geochim. Cosmochim. Acta* **73**, 1970–1999.

Cioflica G., Vlad S., Volanschi E. and Stoici S. (1977) Magnesian skarns and associated mineralization at Baita Bihor. *St. Cerc. Geol. Geofiz. Geogr. Ser. Geol.* **22**, 39–57 (in Romanian).

Clark A. H. (1970) Arsenian sphalerite from Mina Alcarán, Pampa Larga, Copiapó, Chile. *Am. Mineral.* **55**, 1794–1797.

Cook N. J. (1997) Bismuth and bismuth–antimony sulphosalts from Neogene vein mineralisation, Baia Borşa area, Maramureş, Romania. *Mineral. Mag.* **61**, 387–409.

Cook N. J. and Ciobanu C. L. (2001) Paragenesis of Cu–Fe ores from Ocna de Fier-Dognecea (Romania), typifying fluid plume mineralisation in a proximal skarn setting. *Mineral. Mag.* **65**, 351–372.

Cook N. J. and Ciobanu C. L. (2003a) Cervelleite, Ag_4TeS, from three localities in Romania, substitution of Cu, and the occurrence of the associated phase, Ag_2Cu_2TeS. *Neues Jb. Mineral. Monatsh.*, 321–336.

Cook N. J. and Ciobanu C. L. (2003b) Lamellar minerals of the cuprobismutite series and related padraite: a new occurrence and implications. *Can. Mineral.* **41**, 441–456.

Cook N. J. and Ciobanu C. L. (2004) Bismuth tellurides and sulphosalts from the Larga hydrothermal system, Metaliferi Mts., Romania: paragenesis and genetic significance. *Mineral. Mag.* **68**, 301–321.

Cook N. J., Klemd R. and Okrusch M. (1994) Sulphide mineralogy, metamorphism and deformation in the Matchless massive sulphide deposit, Namibia. *Mineral. Deposita* **29**, 1–15.

Cook N. J., Ciobanu C. L. and Mao J. W. (2009) Textural control on gold distribution in As-free pyrite from the Dongping, Huangtuliang and Hougou gold deposits, North China Craton, (Hebei Province, China). *Chem. Geol.* **204**, 101–121.

Craig J. R. (1973) The Cu–Zn–S system. *Mineral. Deposita* **8**, 81–91.

Danyushevsky L., Robinson P., McGoldrick P., Large R. and Gilbert S. (2003) LA-ICPMS of sulphides: evaluation of an XRF glass disc standard for analysis of different sulphide matrixes. *Geochim. Cosmochim. Acta* **67**(18), A73.

Danyushevsky L. V., Robinson P., Gilbert S., Norman M., Large R., McGoldrick P. and Shelley J. M. G. (in press) A technique for routine quantitative multi-element analysis of sulphide minerals by laser ablation ICP-MS. *Geochem.: Explor. Environ. Anal.*

Di Benedetto F., Bernardini G. P., Costagliola P., Plant D. and Vaughan D. J. (2005) Compositional zoning in sphalerite crystals. *Am. Mineral.* **90**, 1384–1392.

Emslie D. P. and Beukes G. J. (1981) Minor- and trace-element distribution in sphalerite and galena from the Otavi Mountainland, South West Africa. *Ann. Geol. Surv. Rep. S. Africa* **15**(2), 11–28.

Epple M., Panthöfer M., Walther R. and Deiseroth H.-J. (2000) Crystal-chemical characterization of mixed valence indium chalcogenides by X-ray absorption spectroscopy (EXAFS). *Z. Krist* **215**, 445–453.

Flood B. (1969) Sulphide mineralizations within the Hecla Hoel complex in Vestspitsbergen and Bjørnøya. Norsk Polarinstitutt Årbok for 1967.

Fowler A. D. and L'Heureux I. (1996) Self-organized banded sphalerite and branching galena in the Pine Point ore deposit, Northwest Territories. *Can. Mineral.* **34**, 1211–1222.

Gottesmann W. and Kampe A. (2007) Zn/Cd ratios in calcsilicate-hosted sphalerite ores at Tumurtijn-ovoo, Mongolia. *Chem. Erde – Geochem.* **67**, 323–328.

Gottesmann W., Gottesmann B. and Seifert W. (2009) Sphalerite composition and ore genesis at the Tumurtjin-ovoo Fe–Mn–Zn skarn deposit, Mongolia. *Neues Jb. Mineral. Abh.* **185**, 249–280.

Graeser S. (1969) Minor elements in sphalerite and galena from Binnatal. *Contrib. Mineral. Petrol.* **24**, 156–163.

Grammatikopoulos T. A., Valeyev O. and Roth T. (2006) Compositional variation in Hg-bearing sphalerite from the polymetallic Eskay Creek deposit, British Columbia, Canada. *Chem. Erde – Geochem.* **66**, 307–314.

Grip E. (1978) Central Sweden (Bergslagen). In *Mineral Deposits of Europe. l. Northwest Europe* (eds. S. H. U. Bowie, A. Kvalheim and H. W. Haslam). Inst. Mining Metall, London.

Harmer S. L., Goncharova L. V., Kolarova R., Lennard W. N., Muñoz-Márquez M. A., Mitchell I. V. and Nesbitt H. W. (2007) Surface structure of sphalerite studied by medium energy ion scattering and XPS. *Surf. Sci.* **601**, 352–361.

Hedström P., Simeonov A. and Malmström L. (1989) The Zinkgruvan ore deposit, south-central Sweden; a Proterozoic, proximal Zn–Pb–Ag deposit in distal volcanic facies. *Econ. Geol.* **84**, 1235–1261.

Höll R., Kling M. and Schroll E. (2007) Metallogenesis of germanium – a review. *Ore Geol. Rev.* **30**, 145–180.

Hofmann C. and Henn U. (1984) Grune Sphalerit aus Zaire. *Z. Deutsche Gemmolog. Gesellsch.* **33**(1–2), 72–74.

Hotje U., Rose C. and Binnewies M. (2003) Lattice constants and molar volume in the system ZnS, ZnSe, CdS, CdSe. *Solid State Sci.* **5**, 1259–1262.

Howard, W. R. (2007) Structural setting and geochemical correlations in bismuth (sulfo) telluride – native gold-bearing veins, CLY Group, British Columbia, Canada: a reduced intrusion-related gold system. Field workshop of IGCP-486, Espoo, Finland, Proceedings Volume. Geol. Surv. Finland Opas **53**, 45–50.

Hurley T. D. and Crocket J. H. (1985) A gold–sphalerite association in a volcanogenic base-metal-sulfide deposit near Tilt Cove, Newfoundland. *Can. Mineral.* **23**, 423–430.

Huston D. L., Sie S. H., Suter G. F., Cooke D. R. and Both R. A. (1995) Trace elements in sulfide minerals from eastern Australian volcanic-hosted massive sulfide deposits; Part I, Proton microprobe analyses of pyrite, chalcopyrite, and sphalerite, and Part II, Selenium levels in pyrite; comparison with delta ^{34}S values and implications for the source of sulfur in volcanogenic hydrothermal systems. *Econ. Geol.* **90**, 1167–1196.

Huston D. L., Jablonsky W. and Sie S. H. (1996) The distribution and mineral hosts of silver in Eastern Australian volcanogenic massive sulfide deposits. *Can. Mineral.* **34**, 529–546.

Intiomale M. M. and Oosterbosch R. (1974) Geologie et geochimie du gisement de Kipushi, Zaire. In *Gisements Stratiformes et Provinces Cupriferes* (ed. P. Bartholome). Soc. Geol. Belg., Liege, pp. 123–164.

Ishihara S. and Endo Y. (2007) Indium and other trace elements in volcanogenic massive sulphide ores from the Kuroko, Besshi and other types in Japan. *Bull. Geol. Surv. Jpn.* **58**, 7–22.

Ishihara S., Hoshino K., Murakami H. and Endo Y. (2006) Resource evaluation and some genetic aspects of indium in the Japanese ore deposits. *Resour. Geol.* **56**, 347–364.

Johan Z. (1988) Indium and germanium in the structure of sphalerite: an example of coupled substitution with copper. *Mineral. Petrol.* **39**, 211–229.

Johan Z. and Oudin E. (1986) Présence de grenats, $Ca_3Ga_2(GeO_4)_3$, $Ca_3Al_2((Ge, Si)O_4)_3$ et d'un équivalent ferrifère, germanifère et gallifère de la sapphirine, $Fe_4(Ga, Sn, Fe)_4(Ga, Ge)_6O_{20}$, dans la blende des gisements de la zone axiale pyrénéenne. Conditions de la formation des phases germanifères et gallifères. *C. R. Acad. Sci. Ser. IIA* **303**, 811–816.

Johan Z., Oudin E. and Picot P. (1983) Analogues germanifères et gallifères des silicates et oxydes dans les gisements de zinc des Pyrénées centrales, France. argutite et carboirite, deux nouvelles espèces minerales. *Tscherm. Mineral. Petrogr. Mitt.* **31**, 97–119.

Kaneko S., Aoki H., Nonaka I., Imoto F. and Matsumoto K. (1984) Solid solution and phase transformation in the system ZnS–MnS under hydrothermal conditions. *J. Electrochem. Soc.* **130**, 2487–2489.

Kato A. (1965) Sakuraiite, a new mineral. *Chigaku Kenkyu (Earth Science Studies)*, Sakurai volume, 1–5 (in Japanese).

Katsev S., L'Heureux I. and Fowler A. D. (2001) Mechanism and duration of banding in Mississippi Valley-type sphalerite. *Geophys. Res. Lett.* **28**, 4643–4646.

Kelley K. D., Leach D. L., Johnson C. A., Clark J. L., Fayek M., Slack J. F., Anderson V. M., Ayuso L. E. and Ridley W. I. (2004) Textural, compositional, and sulfur isotope variations of sulfide minerals in the Red Dog Zn–Pb–Ag deposits, Brooks Range, Alaska: implications for ore formation. *Econ. Geol.* **99**, 1509–1532.

Kissin S. A. and Owens D. R. (1986) The crystallography of sakuraiite. *Can. Mineral.* **24**, 679–683.

Kojima S. and Sugaki A. (1984) Phase relations in the central portion of the Cu–Fe–Zn–S system between 800 and 500 °C. *Mineral. J.* **12**, 15–28.

Kossoff D., Hudson-Edwards K. A., Dubbin W. E. and Alfredsson M. (2008) Incongruent weathering of Cd and Zn from mine tailings. *Mineral. Mag.* **72**, 81–84.

Krämer V., Hirth H., Hofherr M. and Trah H.-P. (1987) Phase studies in the systems Ag_2Te–Ga_2Te_3, ZnSe–In_2Se_3 and ZnS–Ga_2S_3. *Thermochim. Acta* **112**, 89–94.

Kuhlemann J., Vennemann T., Herlec U., Zeeh S. and Bechstädt T. (2001) Variations of sulfur isotopes, trace element compositions, and cathodoluminescense of Mississippi Valley-type Pb–Zn ores from the Drau range, Eastern Alps (Slovenia-Austria): implications for ore deposition on a regional versus microscale. *Econ. Geol.* **96**, 1931–1941.

Kunugiza K. (1999) Incipient stage of ore formation process of the Kamioka Zn–Pb ore deposit in the Hida Metamorphic Belt, Central Japan: leaching and precipitation of clinopyroxene. *Resour. Geol.* **49**, 199–212.

Lepetit P., Bente K., Doering T. and Luckhaus S. (2003) Crystal chemistry of Fe-containing sphalerites. *Phys. Chem. Miner.* **30**, 185–191.

Lombaard A. F., Günzel A., Innes J. and Krüger T. L. (1986) The Tsumeb lead–copper–zinc–silver deposit, South West Africa/Namibia. In *Mineral deposits of Southern Africa*, vol. 2 (eds. C. R. Anhaeusser and S. Maske). Geol. Soc. South Africa, Johannesburg, pp. 1761–1782.

Longerich H. P., Jackson S. E. and Gunther D. (1996) Laser ablation inductively coupled plasma mass spectrometric transient signal data acquisition and analyte concentration calculation. *J. Anal. Atom. Spectrom.* **11**, 899–904.

Lusk J. and Ford C. E. (1978) Experimental extension of the sphalerite geobarometer to 10 kbar. *Am. Mineral.* **63**, 516–519.

Lusk J., Scott S. D. and Ford C. E. (1993) Phase relations in the Fe–Zn–S system to 5 Kbars and temperatures between 325 and 150 °C. *Econ. Geol.* **88**, 1880–1903.

Marshall B. and Gilligan L. B. (1987) An introduction to remobilization: information from ore-body geometry and experimental considerations. *Ore Geol. Rev.* **2**, 87–131.

Martín J. D. and Gil A. S. I. (2005) An integrated thermodynamic mixing model for sphalerite geobarometry from 300 to 850 °C and up to 1 GPa. *Geochim. Cosmochim. Acta* **69**, 995–1006.

Melcher F., Oberthür T. and Rammlmair D. (2006) Geochemical and mineralogical distribution of germanium in the Khusib Springs Cu–Zn–Pb–Ag sulfide deposit, Otavi Mountain Land, Namibia. *Ore Geol. Rev.* **28**, 32–56.

Minčeva-Stefanova J. (1993) A morphological SEM study of wurtzite–sphalerite relationships in specimens from Zvezdel, Bulgaria. *Miner. Petrol.* **49**, 119–126.

Mladenova V. and Valchev S. (1998) Ga/Ge ratio in sphalerite from the carbonate-hosted Sedmochislenitsi Deposit as a temperature indication of initial fluids. *Spis. Bulgar. Geol. Druzh.* **59**(2–3), 49–54.

Moh G. (1975) Tin-containing mineral systems. Part II: Phase relations and mineral assemblages in the Cu–Fe–Zn–Sn–S system. *Chem. Erde* **34**, 1–61.

Moh G. H. and Jäger A. (1978) *Phasengleichgewichte des Systems Ge–Pb–Zn–S in Relation zu Germanium-Gehalten alpiner Pb–Zn-Lagerstätten*. Verhandlungen der Geologischen Bundesanstalt Wien 1978. pp. 437–440.

Möller P. (1987) Correlation of homogenization temperatures of accessory minerals from sphalerite-bearing deposits and Ga/Ge model temperatures. *Chem. Geol.* **61**, 153–159.

Möller P. and Dulski P. (1993) Germanium und gallium distibution in sphalerite. In *Formation of Hydrothermal Vein Deposits – Case Study of the Pb-Zn, Barite and Fluorite Deposits of the Harz Mountains. Monograph Series on Mineral Deposits*, vol. 30 (eds. P. Möller and V. Lüders). Bornträger, Berlin-Stuttgart. pp. 189–196.

Monteiro L. V. S., Bettencourt J. S., Juliani C. and de Oliveira T. F. (2006) Geology, petrography, and mineral chemistry of the Vazante non-sulfide and Ambrósia and Fagundes sulfide-rich carbonate-hosted Zn–(Pb) deposits, Minas Gerais, Brazil. *Ore Geol. Rev.* **28**, 201–234.

Moskalyk R. R. (2003) Gallium: the backbone of the electronics industry. *Miner. Eng.* **16**, 921–929.

Murao S., Sie S. H. and Suter G. F. (1996) Distribution of rare metals in Kuroko-type ore: a PIXEPROBE study. *Nucl. Instr. Meth. Phys. Res.* **B109**(110), 627–632.

Murao S., Deb M. and Furuno M. (2008) Mineralogical evolution of indium in high grade tinpolymetallic hydrothermal veins – a comparative study from Tosham, Haryana state, India and Goka, Naegi district, Japan. *Ore Geol. Rev.* **33**, 490–504.

Nitta E., Kimata M., Hoshino M., Echigo T., Hamasaki S., Nishida N., Shimizu M. and Akasaka T. (2007) Crystal chemistry of ZnS minerals formed as high-temperature volcanic sublimates: matraite identical with sphalerite. *J. Miner. Petrol. Sci.* **103**, 145–151.

Nriagu J. O. (1998) History, production, and uses of thallium. In *Thallium in the Environment* (ed. J. O. Nriagu). John Wiley and Sons, Inc., New York, pp. 1–14.

Öhlander B., Müller B., Axelsson M. and Alakangas L. (2007) An attempt to use LA-ICP-SMS to quantify enrichment of trace elements on pyrite surfaces in oxidizing mine tailings. *J. Geochem. Explor.* **92**, 1–12.

Oen I. S., Kager P. and Kieft C. (1980) Oscillatory zoning of a discontinuous solid–solution series. *Am. Mineral.* **65**, 1220–1232.

Oftedahl I. (1940) Untersuchungen über die Nebenbestandteile von Erzmineralien norwegischer zinkblendführender Vorkommen. *Skrift. Norsk Vidensk. Akad. Oslo, Math. Naturv. Kl.* **8**, 1–103.

Ohta E. (1989) Occurrence and chemistry of indium containing minerals from the Toyoha mine, Hokkaido, Japan. *Mining Geol.* **39**, 355–372.

Ohta E. (1991) Polymetallic mineralization at the Toyoha Mine, Hokkaido, Japan. *Mining Geol.* **41**, 279–295.

Ohta E. (1992) Silver mineralization at the Toyoha Mine, Hokkaido, Japan. *Mining Geol.* **42**, 19–32.

Ohta E. (1995) Common features and genesis of tin-polymetallic veins. *Resour. Geol. Spec. Issue* **18**, 187–195.

Olivo G. R. and Gibbs K. (2003) Paragenesis and mineral chemistry of alabandite (MnS) from the Ag-rich Santo-Toribio epithermal deposit, Northern Peru. *Miner. Mag.* **67**, 95–102.

Ono S., Hirai K., Matsueda H. and Kabashima T. (2004) Polymetallic mineralization at the Suttsu vein-type deposit, southwestern Hokkaido, Japan. *Resour. Geol.* **54**, 453–464.

Orberger B., Pasava J., Gallien J.-P., Daudin L. and Trocellier P. (2003) Se, As, Mo, Ag, Cd, In, Sb, Pt, Au, Tl, Re traces in biogenic and abiogenic sulfides from Black Shales (Selwyn Basin, Yukon territories, Canada): a nuclear microprobe study. *Nucl. Instr. Meth. Phys. Res.* **B210**, 441–448.

Parasyuk O. V., Voronyuk S. V., Gulay L. D., Davidyuk G. Y. and Halka V. O. (2003) Phase diagram of the CuInS–ZnS system and some physical properties of solid solutions phases. *J. Alloys Compd.* **348**, 57–64.

Pattrick R. A. D., Dorling M. and Polya D. A. (1993) TEM study of indium- and copper-bearing growth-banded sphalerite. *Can. Mineral.* **31**, 105–117.

Piatak N. M., Seal, II, R. R. and Hammarstrom J. M. (2004) Environmental significance of cadmium and other trace-element concentrations in sphalerite from mineral deposits. *Geol. Soc. Am. Abstr. Progr.* **36**(5), 27.

Pimminger M., Grasserbauer M., Schroll E. and Cerny I. (1985) Trace element distribution in sphalerites from Pb–Zn ore occurrences of the Eastern Alps. *Tschermaks Mineral. Petrograph. Mitt.* **34**, 131–141.

Pirri I. V. (2002) On the occurrence of selenium in sulfides of the ore deposit of Baccu Locci (Gerrei, SE Sardinia). *N. Jb. Mineral. Monatsh.*, 207–224.

Pósfai M. and Buseck P. R. (1997) Modular structures in sulphides: sphalerite/wurtzite-, pyrite/marcasite-, and pyrrhotite-type minerals. In *Modular Aspects of Minerals EMU Notes in Mineralogy*, vol. 1 (ed. S. Merlino). Eötvös University Press, Budapest, Hungary, pp. 193–235.

Pring A., Tarantino S. C., Tenailleau C., Etchmann B., Carpenter M. A., Zhang M., Liu Y. and Withers R. L. (2008) The crystal chemistry of Fe-bearing sphalerites: an infrared spectroscopic study. *Am. Mineral.* **93**, 591–597.

Putnis A. (2002) Mineral replacement reactions: from macroscopic observations to microscopic mechanisms. *Miner. Mag.* **66**, 689–708.

Qian X. (1987) Trace elements in galena and sphalerite and their geochemical significance in distinguishing the genetic types of Pb–Zn ore deposits. *Chin. J. Geochem.* **6**, 177–190.

Rager H., Amthauer G., Bernroider M. and Schurmann K. (1996) Colour, crystal chemistry, and mineral association of a green sphalerite from Steinperf, Dill Syncline, FRG. *Eur. J. Mineral.* **8**, 1191–1198.

Rambaldi E. R., Rajan R. S., Housley R. M. and Wang D. (1986) Gallium-bearing sphalerite in a metal-sulfide nodule of the Qingzhen (EH3) chondrite. *Meteoritics* **21**, 23–31.

Saini-Eidukat B., Melcher F. and Lodziak J. (2009) Zinc–germanium ores of the Tres Marias Mine, Chihuahua, Mexico. *Miner. Deposita* **44**, 363–370.

Schorr S. and Wagner G. (2005) Structure and phase relations of the Zn[2x](CuIn)[1 − x]S[2] solid solution series. *J. Alloys Compd.* **396**, 202–207.

Schroll E. (1996) *The Triassic carbonate-hosted Pb–Zn mineralisation in the Alps (Europe): the genetic position of Bleiberg type deposits*. Society of Economic Geologists Special Publication 4, pp. 182–194.

Schroll E. (1997) Geochemische und geochronologische Daten und Erläuterungen. In *Handbuch der Lagerstätten der Erze, Industrieminerale und Energierohstoffe Österreichs* (ed. L. Weber). Archiv für Lagerstättenforschung Band 19, Geologische Bundesanstalt Wien. pp. 395–542.

Schwartz M. O. (2000) Cadmium in zinc deposits: economic geology of a polluting element. *Int. Geol. Rev.* **42**, 445–469.

Schwarz-Schampera U. and Herzig P. M. (2002) *Indium: Geology, Mineralogy, and Economics*. Springer, 257pp..

Scott S. D. (1973) Experimental calibration of the sphalerite geobarometer. *Econ. Geol.* **68**, 466–474.

Scott S. D. and Barnes H. L. (1971) Sphalerite geothermometry and geobarometry. *Econ. Geol.* **66**, 653–669.

Segalstad T. V. and Telstø L. (2002) Mineraldannelsen i Konnerudkollen gruver. *Bergverksmuseet Skrift.* **20**, 35–49.

Seifert T. and Sandmann D. (2006) Mineralogy and geochemistry of indium-bearing polymetallic vein-type deposits: implications for host minerals from the Freiberg district, Eastern Erzgebirge, Germany. *Ore Geol. Rev.* **28**, 1–31.

Shimizu M. and Shikazono N. (1985) Iron and zinc partitioning between coexisting stannite and sphalerite: a possible indicator of temperature and sulfur fugacity. *Mineral. Deposita* **20**, 314–320.

Shimizu M., Kato A. and Shiozawa T. (1986) Sakuraiite: chemical composition and extent of (Zn–Fe)In– for –Cu–Sn substitution. *Can. Mineral.* **24**, 405–409.

Shimizu M., Matsubara S., Shimizu M., Kyouno Y., Harada A. and Cook N. J. (2007) High-grade Ag–Cu–Sn–In mineralization in the Nishizawa-Ashio area, Tochigi Prefecture, central Japan. *Geochim. Cosmochim. Acta* **71**(Suppl. 1), A930.

Sinclair W. D., Kooiman G. J. A., Martin D. A. and Kjarsgaard I. M. (2006) Geology, geochemistry and mineralogy of indium resources at Mount Pleasant, New Brunswick, Canada. *Ore Geol. Rev.* **28**, 123–145.

Sombuthawee C., Bonsall S. B. and Hummel F. A. (1978) Phase equilibria in the systems ZnS–MnS, ZnS–CuInS, and MnS–CuInS. *J. Solid State Chem.* **25**, 391–399.

Sombuthawee C. and Hummel F. A. (1979) Subsolidus equilibria in the system ZnS–MnS–$CuInS_2$. *J. Solid State Chem.* **30**, 125–128.

Sugaki A., Kitakaze A. and Kojima S. (1987) Bulk compositions of intimate intergrowths of chalcopyrite and sphalerite and their genetic implications. *Miner. Deposita* **22**, 26–32.

Sundblad K. (1994) A genetic reinterpretation of the Falun and Åmmeberg ore types, Bergslagen, Sweden. *Miner. Deposita* **29**, 170–179.

Tamas C. G., Bailly L., Ghergari L., O'Connor G. and Minut A. (2006) New occurrences of tellurides and argyrodite in Rosia Montana, Apuseni Mountains, Romania, and their metallogenic significance. *Can. Mineral.* **44**, 367–383.

Taylor C. M. and Radtke A. S. (1969) Micromineralogy of silver-bearing sphalerite from Flat River, Missouri. *Econ. Geol.* **64**, 306–318.

Tomashik V. N., Oleinik G. S. and Mizetskaya I. B. (1978) The ternary mutual system CdTe + ZnS = CdS + ZnTe. *Inorg. Mater.* **14**, 1428.

Ueno T. and Scott S. D. (1991) Solubility of gallium in sphalerite and wurtzite at 800 degrees C and 900 degrees C. *Can. Mineral.* **29**, 143–148.

Vaughan D. J. and Rosso K. M. (2006) Chemical bonding in sulfide minerals. In *Sulfide Mineralogy and Geochemistry* (ed. D. J. Vaughan). *Rev. Mineral. Geochem.* **61**, pp. 231–264.

Viets J. G., Hopkins R. T. and Miller B. M. (1992) Variations in minor and trace metals in sphalerite from Mississippi Valley-type deposits of the Ozark region: genetic implications. *Econ. Geol.* **87**, 1897–1905.

Watanabe Y. (1990) Pull-apart vein system of the Toyoha deposit, the most productive Ag–Pb–Zn vein-type deposit in Japan. *Mining Geol.* **40**, 269–278.

Watanabe Y. and Ohta E. (1995) The relation of two-stage mineralization at the Ag–Pb–Zn Toyoha deposit, Southwest Hokkaido, to subduction of the Pacific Plate. *Resour. Geol. Spec. Issue* **18**, 197–202.

Watling R. J., Herbert H. K. and Abell I. D. (1995) The application of laser ablation-inductively coupled plasma-mass spectrometry (LA-ICP-MS) to the analysis of selected sulphide minerals. *Chem. Geol.* **124**, 67–81.

Weisener C., Smart R. and Gerson A. (2004) A comparison of the kinetics and mechanism of acid leaching of sphalerite containing low and high concentrations of iron. *Internat. J. Miner. Process.* **74**, 239–249.

Wu P., Kershaw R., Dwight K. and Wold A. (1989) Growth and characterization of nickel-doped ZnS single crystals. *Mater. Res. Bull.* **24**, 49–53.

Xiong Y. (2007) Hydrothermal thallium mineralization up to 300 °C: a thermodynamic approach. *Ore Geol. Rev.* **32**, 291–313.

Associate editor: David J. Vaughan